Resource

Cell Metabolism

A Strategy for Discovery of Endocrine Interactions with Application to Whole-Body Metabolism

Graphical Abstract

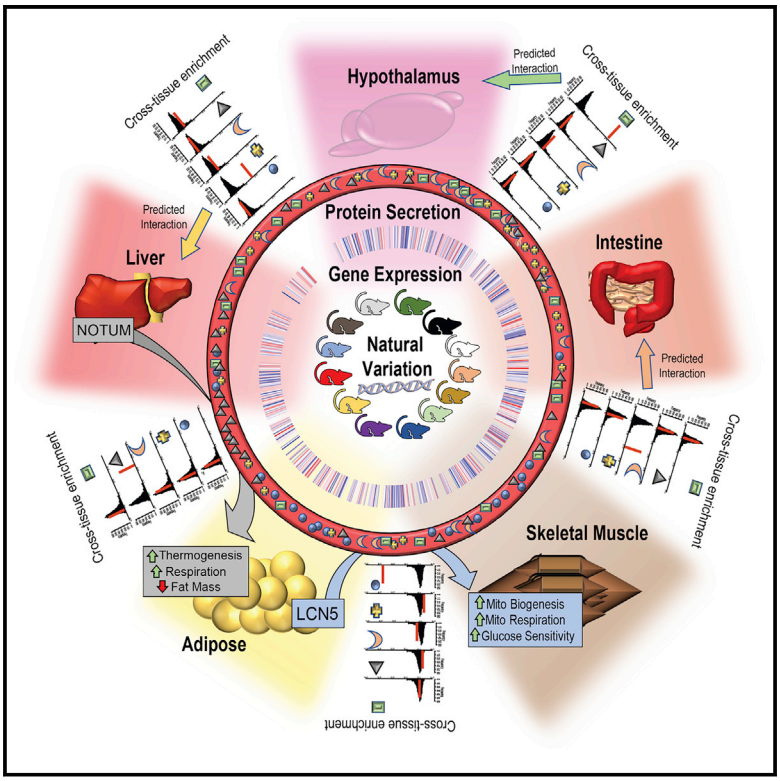

Highlights

- A population-based method to discover novel endocrine factors using expression data
- Discovery that adipose-derived mouse LCN5/human LCN6 enhances muscle respiration
- Discovery that liver-derived NOTUM promotes adipose tissue thermogenesis
- Significant overlap of predictions between mouse and human endocrine interactions

Authors

Marcus M. Seldin, Simon Koplev, Prashant Rajbhandari, ..., Rita M. Cantor, Johan L.M. Björkegren, Aldons J. Lusis

Correspondence

jlusis@mednet.ucla.edu

In Brief

Seldin and colleagues use a bioinformatics-based approach to identify new inter-tissue endocrine circuits. Using this resource, they report on two novel endocrine factors—adipose-derived Lipocalin-5, which promotes muscle mitochondrial respiration, and liver-secreted Notum, which mediates adipose tissue beiging.

Seldin et al., 2018, Cell Metabolism *27*, 1138–1155
May 1, 2018
https://doi.org/10.1016/j.cmet.2018.03.015

CellPress

CellPress

Cell Metabolism
Resource

A Strategy for Discovery of Endocrine Interactions with Application to Whole-Body Metabolism

Marcus M. Seldin,[1] Simon Koplev,[2,3] Prashant Rajbhandari,[4] Laurent Vergnes,[5] Gregory M. Rosenberg,[1] Yonghong Meng,[1] Calvin Pan,[1,5] Thuy M.N. Phuong,[1] Raffi Gharakhanian,[1] Nam Che,[1] Selina Mäkinen,[7,12] Diana M. Shih,[1] Mete Civelek,[8] Brian W. Parks,[9] Eric D. Kim,[1] Frode Norheim,[10] Karthickeyan Chella Krishnan,[1] Yehudit Hasin-Brumshtein,[1] Margarete Mehrabian,[1] Markku Laakso,[11] Christian A. Drevon,[10] Heikki A. Koistinen,[7,12] Peter Tontonoz,[4] Karen Reue,[5] Rita M. Cantor,[5] Johan L.M. Björkegren,[2,3] and Aldons J. Lusis[1,5,6,13,*]

[1]Department of Medicine, University of California, Los Angeles, Los Angeles, CA, USA
[2]Department of Genetics and Genomic Sciences, The Icahn Institute for Genomics and Multiscale Biology, Icahn School of Medicine at Mount Sinai, New York, NY, USA
[3]Integrated Cardio Metabolic Centre, Department of Medicine, Karolinska Institutet, Karolinska Universitetssjukhuset, Huddinge, Sweden
[4]Department of Pathology and Laboratory Medicine, University of California, Los Angeles, Los Angeles, CA, USA
[5]Department of Human Genetics, University of California, Los Angeles, Los Angeles, CA, USA
[6]Department of Microbiology, Immunology and Molecular Genetics, University of California, Los Angeles, CA, USA
[7]Department of Medicine, University of Helsinki and Helsinki University Central Hospital, Helsinki, Finland
[8]Department of Biomedical Engineering, University of Virginia, Charlottesville, VA, USA
[9]Department of Nutritional Sciences, University of Wisconsin, Madison, WI, USA
[10]Department of Nutrition, Institute of Basic Medical Sciences, Faculty of Medicine, University of Oslo, Oslo, Norway
[11]Institute of Clinical Medicine, Internal Medicine, University of Eastern Finland and Kuopio University Hospital, Kuopio, Finland
[12]Minerva Foundation Institute for Medical Research, Biomedicum 2U, Helsinki, Finland
[13]Lead Contact
*Correspondence: jlusis@mednet.ucla.edu
https://doi.org/10.1016/j.cmet.2018.03.015

SUMMARY

Inter-tissue communication via secreted proteins has been established as a vital mechanism for proper physiologic homeostasis. Here, we report a bioinformatics framework using a mouse reference population, the Hybrid Mouse Diversity Panel (HMDP), which integrates global multi-tissue expression data and publicly available resources to identify and functionally annotate novel circuits of tissue-tissue communication. We validate this method by showing that we can identify known as well as novel endocrine factors responsible for communication between tissues. We further show the utility of this approach by identification and mechanistic characterization of two new endocrine factors. Adipose-derived Lipocalin-5 is shown to enhance skeletal muscle mitochondrial function, and liver-secreted Notum promotes browning of white adipose tissue, also known as "beiging." We demonstrate the general applicability of the method by providing *in vivo* evidence for three additional novel molecules mediating tissue-tissue interactions.

INTRODUCTION

Multicellular organisms have evolved dynamic means for communication between cell types to maintain proper physiologic homeostasis. In mammals, secreted peptides have been described to regulate nearly all aspects of physiology. Beginning with the discovery of insulin nearly a century ago (Williams, 1993), endocrine tissue crosstalk has been a primary focus for the detection and treatment of adverse metabolic perturbations. Since then, many secreted proteins have been identified that play crucial roles in metabolism (Friedman and Halaas, 1998; Kershaw and Flier, 2004; Salomon et al., 1989; Trujillo and Scherer, 2005), immune system function (Belardelli, 1995; Mosmann and Coffman, 1989), cardiovascular pathobiology (Nian et al., 2004; Tedgui and Mallat, 2006), and many other aspects of physiology. Previous studies have shown that substantial interactions between tissues persist across multiple transcripts in various physiologic states (GTEx Consortium, 2013; Price et al., 2011). Even for autonomous cells such as bacteria, mechanisms have been identified by which secreted components relay signals from one cell to another (Miller and Bassler, 2001). Regardless of the total cell number, size, or complexity of species, nearly all organisms have maintained a capacity to communicate by means of secreted polypeptides throughout evolution. Current estimates in mice and humans predict that roughly ~3,000 unique proteins are secreted, accounting for ~16% of the entire protein coding genome (Lindskog, 2015; Uhlen et al., 2010), and recent studies have provided convincing evidence that microRNAs can also mediate inter-tissue communication (Thomou et al., 2017).

Advances in "omics" technologies such as shotgun proteomics and RNA sequencing (RNA-seq) have enabled unbiased discovery of many additional systemic regulators of whole-body homeostasis (Civelek and Lusis, 2014; Gehlenborg et al., 2010; Joyce and Palsson, 2006; Kussmann et al., 2006). Substantial efforts have been dedicated to assessing single-cell- or tissue-specific secretome through proteomics analysis of

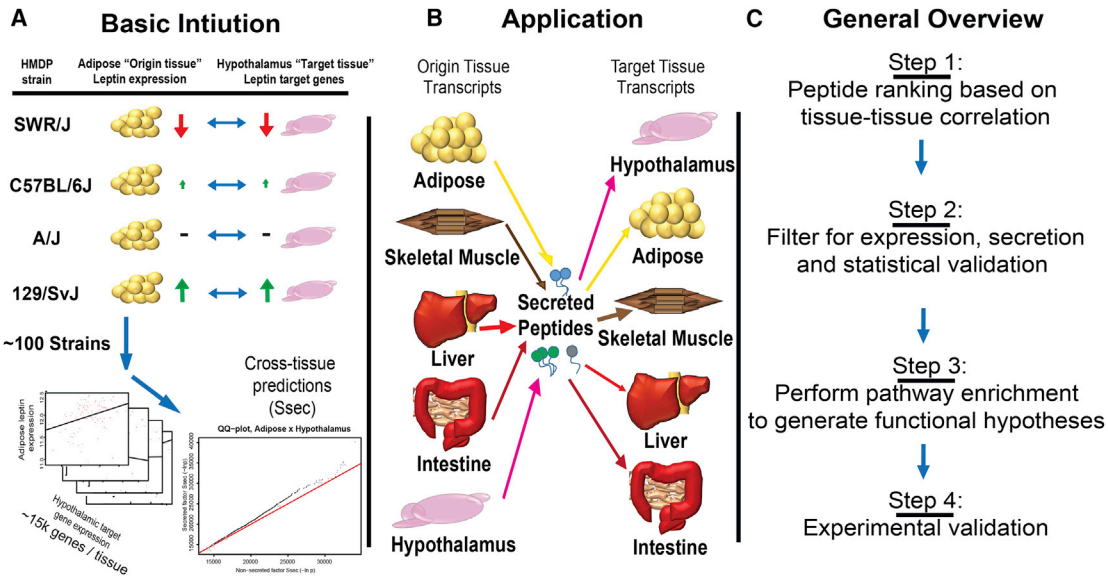

Figure 1. Annotated Schematic for QENIE

(A) The basic intuition for our approach is illustrated for four strains where adipose tissue expression of *Leptin* varies in a manner consistent with hypothalamus target genes. When applied to ~100 HMDP strains, this correlation of gene expression is used for cross-tissue predictions.

(B) This framework was applied to 5 tissues, each examined for gene expression using ~20,000 probes corresponding to ~15,000 genes or RNA-seq in 106 inbred strains of mice. We assigned each axis for every combination of "origin" and "target" tissues.

(C) Generalized steps for method progression and the application, discussed on greater detail in the main text.

cultured medium (Alvarez-Llamas et al., 2007; Hathout, 2007; Katz-Jaffe et al., 2009) and to filtering transcriptomic data for the presence of signal peptides for secretion (Hathout, 2007; Mosquera et al., 2009; Nielsen et al., 1997). Similarly, serum has been subjected to mass spectrometry proteomics in order to identify candidate molecules involved in inter-tissue communication, focusing on biomarker identification (Hathout, 2007; Lawlor et al., 2009; Makridakis and Vlahou, 2010; Petricoin and Liotta, 2004). More advanced approaches have shown differential networks of gene expression across tissues (Keller et al., 2008; Pierson et al., 2015), and even tissue-specific networks to suggest individual genes regulating these axes (Long et al., 2016). One important component lacking in these approaches, however, is the ability to gain insight about the function, mechanism of action, and specific target tissue(s) of identified secreted proteins. In general, uncovering the physiologic functions of endocrine and paracrine polypeptides requires costly and time-consuming biochemical experimentation.

Here, we report a bioinformatics framework that uses natural variation in transcript levels across tissues in a population to identify and functionally annotate endocrine circuits. This method, termed Quantitative Endocrine Network Interaction Estimation (QENIE), can be applied to any collection of organs, tissues, or cell types sampled from a genetically diverse population and profiled using omics platforms. Many of the top-ranked candidates for each tissue-tissue axis here already have established mechanisms of endocrine communication, validating the approach. To prioritize putative endocrine factors, we consider relevant physiologic and clinical traits along with publicly available resources on tissue-specific gene expression. These efforts led to the identification of two new endocrine factors. The first is an adipose-derived protein, which enhances skeletal muscle mitochondrial activity resulting in increased lean body mass and improved insulin sensitivity. The second involves a hepatic secreted protein that can promote adipose tissue "beiging," resulting in improved resistance to cold and increased energy expenditure *in vivo*. To demonstrate the general applicability of the approach, we identify and validate *in vivo* three additional secreted molecules involving communication between tissues, adipose, and heart (SPARC-related modular calcium-binding protein 1 [SMOC1] and inter-alpha-trypsin inhibitor heavy chain family member 5 [ITIH5]), and within aorta (platelet basic protein precursor [PPBP]). We also provide evidence for the applicability of the method to human omics data.

RESULTS

The basic intuition for QENIE is as follows: in a population exhibiting natural variation, transcript levels for most genes differ among individuals. Thus, the inter-organ communication between two tissues will vary in a coordinated manner, with differences in expression of an endocrine factor in one tissue showing correlation with the responder genes and pathways in a target tissue. To identify secreted endocrine factors, we screened for correlations by examining global transcript levels between pairs of tissues and filtering for origin (or sender) tissue secretion (Figure 1). Applying this approach to data from a large cohort of inbred strains of mice revealed many previously described endocrine interactions that were consistent with their published functions. For example, in several inbred mouse strains, genetic diversity and gene-by-environment interactions will drive adipose tissue variation in *Leptin* expression. Given the significant

role of *Leptin* in regulating hypothalamus gene expression and function, we expect to observe variation in hypothalamic "target" genes in a manner consistent with the levels of *Leptin* in adipose (Figure 1A). By applying this intuition to a diverse population, we can assess strength of cross-tissue predictions for endocrine circuits, termed S_{sec}. Here, we also uncovered many novel potential circuits for inter-tissue communication (Figure 1B), several of which we experimentally validated.

Transcriptomic Screening for Regulators of Inter-tissue Crosstalk in the HMDP

To uncover secreted proteins that regulate processes in an endocrine fashion, we utilized global transcript levels determined using expression arrays and RNA-seq from five tissues (liver, skeletal muscle, adipose, hypothalamus, and intestine) in 106 common inbred strains of mice that constitute the Hybrid Mouse Diversity Panel (HMDP). Our initial studies were performed with mice fed a high-fat (HF)/high-sucrose (HS) diet (Hasin-Brumshtein et al., 2016; Parks et al., 2013, 2015). A tutorial of our pipeline, pre-treatment of data, datasets used, and R script implemented for each step of this pipeline is provided at: https://github.com/marcus-seldin/QENIE. For every tissue pair, cross-tissue biweight midcorrelation matrices were calculated across mouse strains. This coefficient, termed bicor, is similar to a Pearson's correlation coefficient (typically illustrated as r), but offers the advantage of more robustness due to removal of outliers in a dataset (Langfelder and Horvath, 2012). To assess the significance of the correlations in these matrices, Student's correlation p values were calculated using the bicor coefficient, which minimizes effects due to outliers (Langfelder and Horvath, 2008). For each matrix of tissue-by-tissue p values of associations, individual organs were then designated "origin" or target tissues.

To identify proteins that act in an endocrine fashion for each matrix of correlations, we included only genes for each origin tissue that encode secreted proteins. This was done by overlaying gene symbols with those annotated to be secreted the Universal Protein Resource (UniProt) database (Leinonen et al., 2006; UniProt Consortium, 2015). In total, these annotations contain ~2,300 unique secreted proteins, of which 1,047–1,213 (depending on the tissue) were retained in our expression data as origin tissue genes encoding a secreted protein. The p value matrices of secreted genes were then ranked by the level of significance of association with all target tissues, listed as "step 1: ranking" in Figure 1. This was accomplished by computing the sum of the –ln(p value) for each origin secreted protein across all target tissue transcripts, listed further as S_{sec}. To make the S_{sec} values comparable between various endocrine circuits, this sum of the –ln(p value) was normalized by the total number of target tissue transcripts. We have illustrated an overview of the procedure (Figure S1).

For example, in adipose-to-hypothalamus, the expression of *Leptin* in adipose tissue varies across the mouse population, and shows significant correlation with body weight (Figure 2A), consistent with corresponding positive plasma correlations to body mass index across the human populations (Farooqi and O'Rahilly, 2009; Margetic et al., 2002). The S_{sec} scores for each individual adipose transcript across all hypothalamic transcripts had a skewed distribution toward higher values, indicating physiologically significant interactions (Figure 2B). Leptin ranked at the extreme upper end of all S_{sec} scores, consistent with many previous observations that Leptin exerts a robust impact on hypothalamic gene expression (Elmquist et al., 1998; Schwartz et al., 1996).

The S_{sec} rankings were then filtered ensuring that genes were primarily expressed by the origin tissue. This was accomplished by manual inspection of each gene in multi-tissue expression panels available via BioGPS (Su et al., 2002; Wu et al., 2009) in both mouse and humans (representative examples using BioGPS arrays shown in Figure S3). Genes not detected in BioGPS arrays were investigated for tissue specificity using the UniProt literature query for "tissue specificity." We provide the top five secreted proteins remaining after the tissue-specific filtering for all pairs of adipose, skeletal muscle, hypothalamus, intestine, and liver tissue (Figures 2C–2G). A significant number (44%) of the highest-ranked secreted proteins have previously been implicated as functional contributors to physiology. In Figures 2C–2G, bold text indicates the secreted proteins with an association between SNPs and metabolism-related clinical traits in humans. Also indicated are any published observations in which a secreted protein has been shown to affect its corresponding target tissue, highlighted with a green background. Several notable interactions were identified. For example, Ghrelin (gene symbol *Ghrl*) presents the strongest intestine-to-hypothalamus interaction (Figure 2F), consistent with this hormone functioning as one of the most robust satiety signals (Klok et al., 2007; Lazarczyk et al., 2003). In addition, many well-known adipokines were identified (Figure 2C), including Adiponectin (*Adipoq*) (Kadowaki et al., 2006; Scherer et al., 1995), Angiopoietin-Like 4 (*Angptl4*) (Kersten et al., 2000; Wozniak et al., 2009; Yoshida et al., 2002), Resistin (*Res*) (Kusminski et al., 2005; Steppan et al., 2001), and Retinol binding protein-4 (*Rbp4*) (Graham et al., 2006; Rocchi et al., 1989). To assess the average "level" of communication between tissues, we calculated the mean and SD values for all secreted proteins in the origin tissue and their respective average cross-tissue S_{sec} scores (Figures 2C–2G). Across all tissues, the highest significance of any secreted protein was found between liver and adipose, gauged by the mean and SE of the S_{sec} scores (Figures 2C and 2E). Listed below each tissue-tissue axis in Figure 2, we also provide the number of positive and negative correlations contributing to each circuit. Given that our S_{sec} score is only one example of assessing cross-tissue communication, other strategies could include focusing of direction of correlation, as opposed to level of significance. It is also worth mentioning that, among liver and adipose tissue arrays, we observed concordant cross-tissue S_{sec} scores between sexes among all secreted factors, which was markedly reduced among the top 50 genes for each axis (Figure S3) where we expect the strongest predictive value for endocrine communication. These provide a generalized strategy to identify the strongest sets of tissue-tissue interactions within our dataset.

Top-Ranked Candidate Peptide Significance Scores Reside in the Upper Limits of Distributions of Permuted S_{sec} Calculations

Given that we did not know the distribution of the test statistic tissue-specific expression arrays, we ran permutation tests to estimate the levels of significance for each top-ranked gene for

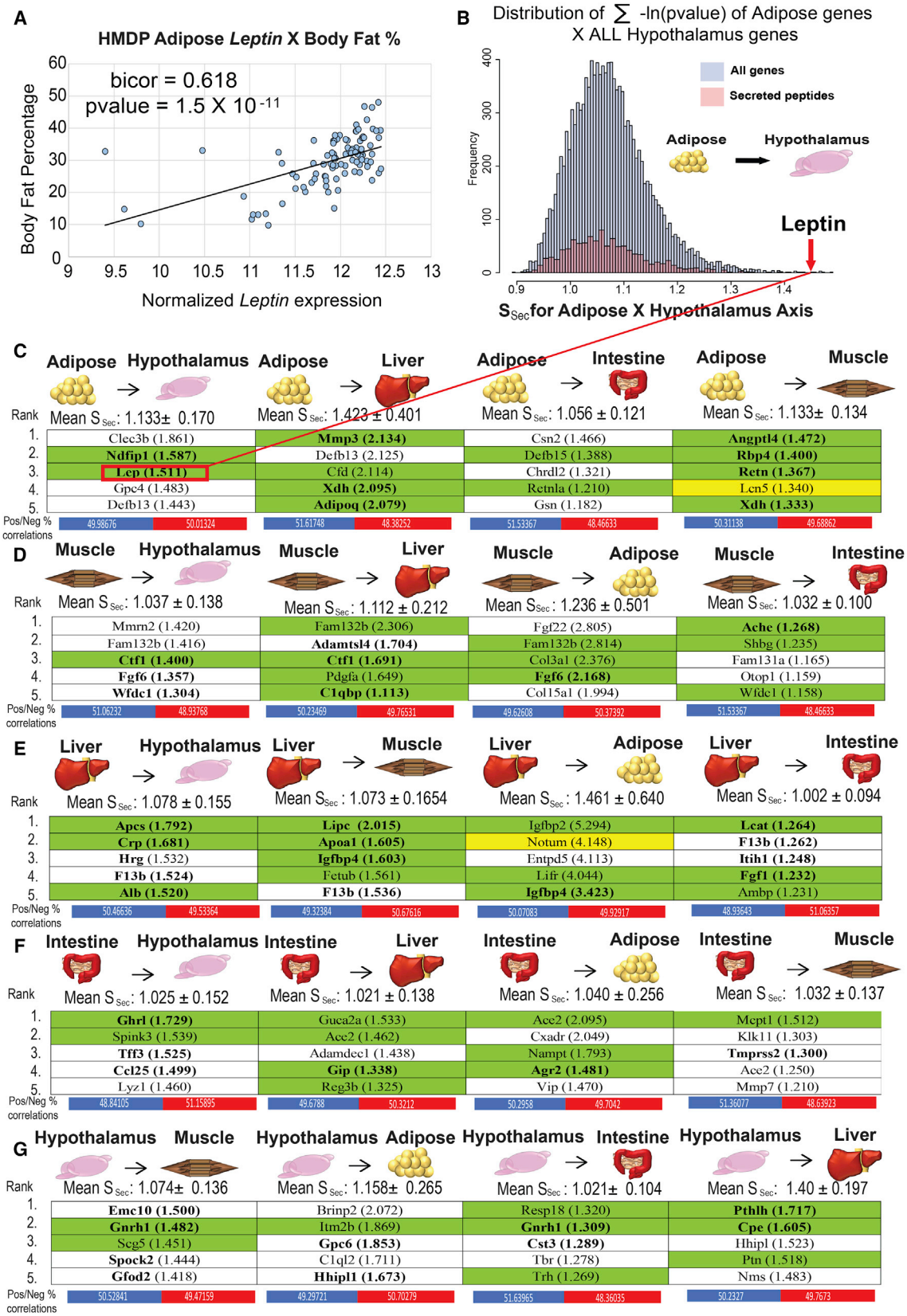

(legend on next page)

every tissue-tissue axis using an adaptive permutation procedure (O'Gorman, 2002), highlighted by green arrows in Figure S1. We permuted the target tissue strains and recalculated S_{sec} to construct the null distribution and maintain the gene-gene correlation structures in each tissue. These tests typically required 1,000–1,000,000 permutations, listed as p values in Table S1. The permutation tests were designed to specifically to allow generation of a statistic while maintaining correlation structure to limit the influence of inflation of cross-tissue gene correlations (discussed below). We note that in these tests the p values used reflect a placeholder for the correlation coefficient, which does not require independence. Beyond permutation testing, we also compared various strategies with rank cross-tissue circuits. An alternative approach to S_{sec} scoring could include counting the number of significant correlations. For the two endocrine circuits explored in-depth (below), we compared the S_{sec} (sum –ln(p value)) with ranking systems generated by counting the total number of significant correlations at various p value cutoffs (Figure S4). These analyses also help to point out that S_{sec} is capturing more of an aggregate of many lower-strength but still significantly correlated genes, as opposed to being driven by fewer highly correlated genes.

To further provide a rationale for focusing on secreted proteins using the S_{sec} ranking system, we compared the relative enrichment of cross-tissue –ln(p value) for all secreted proteins versus genes coding for non-secreted factors. For nearly every inter-organ axis, we observed a higher significance of p values for secreted factors versus non-secreted, most notably within the top percentiles of significance strength (Figure S5). One possible explanation for inter-tissue circuits that showed stronger significance among non-secreted factors (such as muscle-to-adipose) is that we are observing metabolic processes that generate small molecules that act between tissues. In these scenarios, one would expect strong correlations between genes involved in enzymatic production of a metabolite in the origin tissue and genes which utilize or sense the molecule in the target tissue. These observations indicate that, while S_{sec} values for secreted peptides vary across tissues, they are significant for the top-ranked candidates. Using this final list of ranked origin tissue expressed and secreted proteins, and their subsequent target tissue level of statistically validated significance we next focused on functional assessment and specific hypothesis testing of several novel candidates.

Suggestive Pathways Targeted by Inter-tissue Communication and Screening Pipeline for Validation

Ranked lists of genes targeted by potential endocrine proteins were next evaluated for pathway and process enrichment using The Database for Annotation, Visualization and Integrated Discovery (Huang et al., 2007; Sherman et al., 2007). The gene ranks consisted of the top-500 most significantly correlated genes in the target tissue (2%–2.7% of probes on the arrays, discussed in the STAR Methods). In this way, we interrogated cross-tissue enrichment using the gene ontology (GO) Biological Process resource (Ashburner et al., 2000; Gene Ontology Consortium, 2015) and the Kyoto Encyclopedia of Genes and Genomes pathways database (Du et al., 2014; Ogata et al., 1999). Although generally providing broad biological descriptions, the cross-tissue enrichment results nonetheless yielded substantial insight into the likely functions of each secreted protein, thus allowing for effective hypothesis generation.

Implementing these steps generated lists of potential endocrine factors for each tissue-tissue circuit and testable hypotheses with which to follow up. Given that our criteria for validation was based on changes in gene expression in predicted target tissue pathways, we first generated lists of marker genes for each pathway. These genes were chosen based on (1) presence in the top correlated (absolute, positive or negative) genes that were used for pathway prediction and (2) the gene being annotated in the literature as a robust regulator of physiologic process, and, thus, appropriate surrogate for tested functional outcomes.

To functionally validate these factors, we implemented the following experimental approaches: first, cDNA constructs (or GFP control) for each endocrine factor were cloned into an expression plasmid and overexpressed in HEK293 cells. Medium harvested from these cells was used as treatment on target tissue cell types and validated using qPCR. Following up, an epitope-tagged protein from this system was purified from the medium and subsequently used for cell culture treatment or injection into mice. This overall process is illustrated in Figure 3 and summarized from left-to-right panels. First, by screening predicted proteins in various mouse populations with a conditioned medium approach we have observed a roughly 15%–25% success rate depending on the population used. In total, we have screened 36 potential secreted factors via conditioned medium on cell lines reflecting target tissue, and observed 8 in which predicted target genes are significantly altered. Although potential factors that could confound predictions are discussed in detail below, we note that a "negative result" with this artificial system does not mean that a bona fide interaction does not persist, just that gene expression effects were not observed in these specific contexts. A more thorough system to screen factors for physiologic impacts is presented in Figure 3. Here, we applied QENIE to two separate HMDP populations (as opposed to Figure 2), under basal chow conditions (Figures 3A–3F) or a pro-atherosclerotic setting (Figures 3G–3I), and uncovered three

Figure 2. QENIE Application to HMDP Tissues Uncovers Known Regulators of Endocrine Function

(A) Leptin adipose expression in the HMDP correlates with relevant clinical traits consistent with its known function(s).

(B) Distribution of significance score for all adipose genes (blue) and secreted peptides (pink) across all hypothalamic gene expression in 106 strains. Leptin (indicated by arrow) identified as a top-ranked peptide for this axis indicated by red line.

(C–G) Normalized average significance scores and corresponding SDs for each cross-organ combination. Arrows indicate directionality of secreted peptide genes assigned to origin tissues for adipose (C), skeletal muscle (D), liver (E), intestine (F), and hypothalamus (G) across all transcripts in each respective target tissue. Listed are the five highest-ranked origin secreted proteins for each axis, with corresponding mean significance scores in parentheses. Below each axis are the percentiles of positively versus negatively significantly correlated target tissue genes ($p < 0.05$) that contribute to all origin S_{sec} scores. Bold names indicate documented SNPs for the gene associating with a clinical trait, and green backing shows peptides that have been shown to affect function of target tissues. The two genes highlighted with a yellow background are followed up in this study.

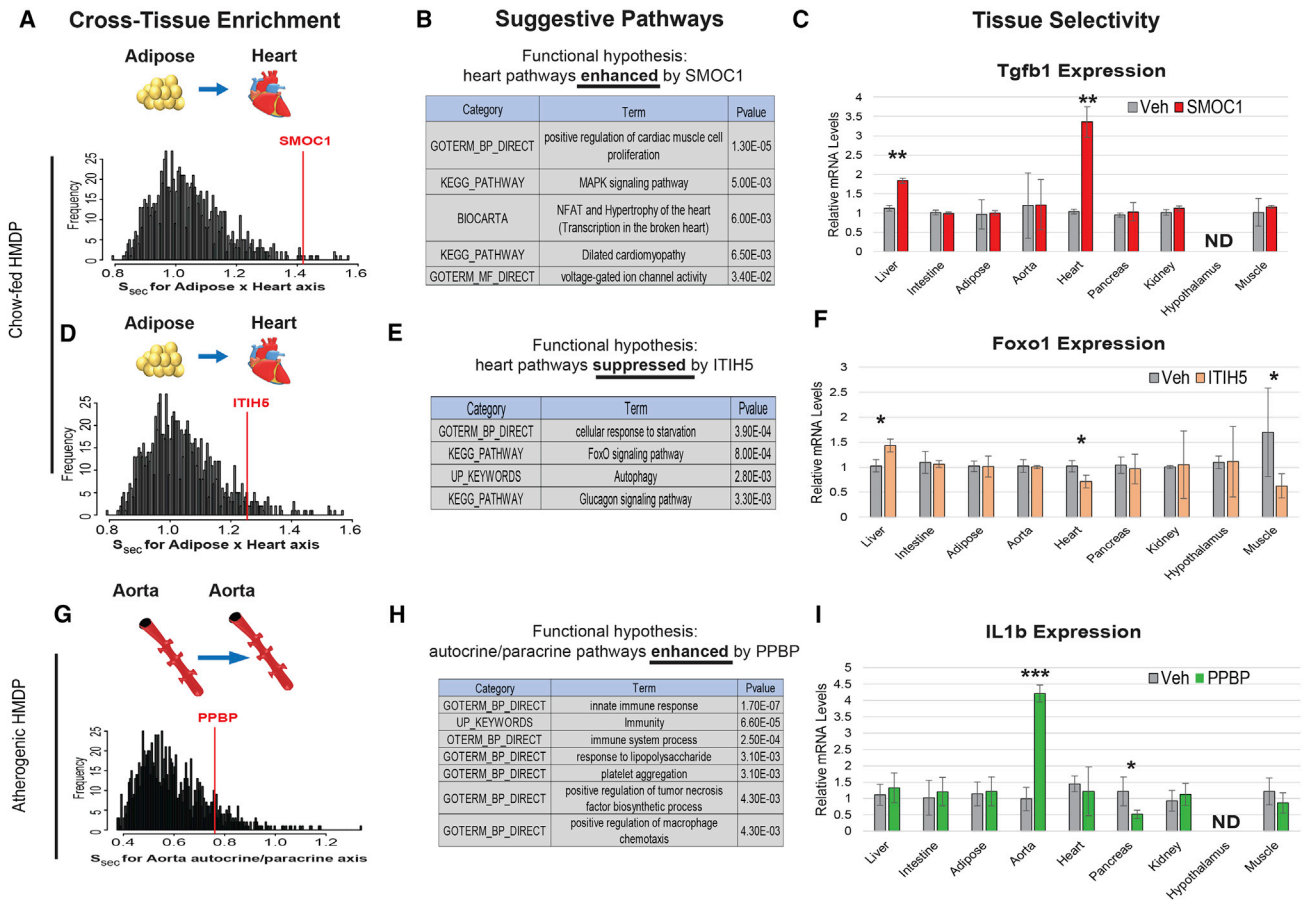

Figure 3. Application of QENIE Is Robust in Identifying Endocrine Factors across Various Datasets

Three additional endocrine factors were screened using the same approach, where the enrichment among all secreted factors is shown for each tissue-tissue axis in various datasets (left), as well as suggestive pathway enrichment based on conditioned correlation coefficients (middle) and tissue specificity of action following injection of recombinant protein (right). By implementing data from a different HMDP cohort on a chow diet, QENIE uncovered SMOC1 (A–C) and ITIH5 (D–F) as adipose-derived regulators of heart *Tgf1b* and *Foxo1*, respectively. Data used from an atherosclerosis-prone mouse population was applied to uncover autocrine/paracrine regulators of aortic gene expression, where *Ppbp* was found to enhance *IL1b* gene expression (G–I). Tissue specificity screening utilized C57BL/6J mice on a chow diet, injected with Veh (saline) or 0.1 μg/g body weight recombinant protein. ND, not detected (assessed by a raw qPCR Ct value above 30). All data presented as means ± SEM *p < 0.05, **p < 0.01, ***p < 0.001.

novel inter-tissue interactions. We note that the factors presented in Figure 3 do not necessarily show the strongest cross-tissue enrichment. These factors were chosen in part based on our own interests. The results suggest that the endocrine interactions persist beyond the upper-limits of the predicted distributions.

Initially, we uncovered the adipokine SMOC1 as a potential regulator of heart muscle proliferation and hypertrophy (Figures 3A–3C). Therefore, we asked whether injection of recombinant SMOC1 could alter a key regulator of muscle cell development and proliferation, transformation growth factor β1 (*Tgfb1*). Here we observed a significant induction of *Tgfb1* in the hearts of SMOC1-injected mice (Figure 3C). We also investigated the potential regulation of other predicted pathways, specifically mitogen-activated protein kinase (MAPK), hypertrophy, and calcium handling. Although we observed changes in calcium-related gene expression (*Cam2k*) in the SMOC1-injected hearts, no changes were observed for *Mapk1* (data not shown). SMOC1 has been demonstrated to regulate developmental processes, specifically BMP antagonism, leading to limb malformations (Okada et al., 2011; Rainger et al., 2011), as well as endothelial TGF-β signaling (Awwad et al., 2015), suggesting that it acts in tissues other than heart.

Another analysis of the same chow-fed dataset uncovered ITIH5 as enriched across the cardiac gene expression profile (Figure 3D). GO showed enrichment for pathways involved in cellular starvation response with ITIH5 as a negative regulator (Figure 3E). In response to injection of recombinant ITIH5, tissue-wide expression analysis showed ITIH5 reduced Forkhead box O1 (*Foxo1*) gene expression in the heart (Figure 3F). Although we did not observe changes in AMPK (*Prkaa1*) in response to the protein injection, other downstream targets, such as acetyl-Co-A carboxylase 1 (*Acc1*) were significantly altered (data not shown). ITIH5 has been shown to affect myofibroblast differentiation (Martin et al., 2016) and implicated as a marker of obesity (Anveden et al., 2012) and several types of

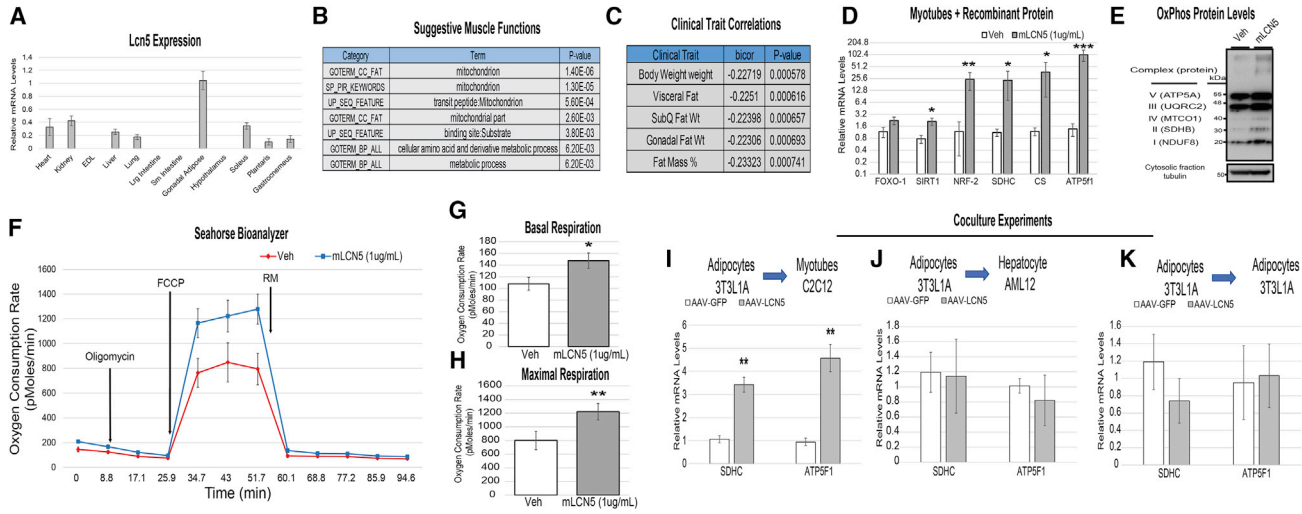

Figure 4. Functional Validation of *Lcn5* as a Regulator of Skeletal Muscle Metabolism *In Vitro*

(A) qPCR analysis of Lcn5 expression across indicated tissues in C57BL/6J mice.

(B) Suggestive pathway enrichment derived from skeletal muscle genes ranked by correlation with adipose *Lcn5*.

(C) Adipose *Lcn5* expression correlation with clinical traits within the HMDP.

(D) C2C12 myotubes were treated overnight with medium containing either PBS (Veh) or recombinant LCN5 protein (1 μg/mL) then subjected to qPCR analysis.

(E–H) The same treatment as in (D) was carried out for 30 hr, then cells were immunoblotted for respiratory complex abundance (E) or subjected to Seahorse bioanalyzer (F) to assess oxygen consumption in both basal (G) and maximal respiratory (H) conditions. For Seahorse experiments, oxygen consumption was normalized to total protein content.

(I–K) 3T3l1 pre-adipocytes infected with either AAV-GFP or AAV-LCN5 were differentiated and placed in co-cultures with C2C12 myotubes (I), AML12 hepatocytes (J), or 3T3L1 adipocytes (J) for 24 hr and qPCR-probed for *Sdhc* or *Atp5f1*. n = 4–8 per group. All data presented as means ± SEM *p < 0.05, **p < 0.01, ***p < 0.001.

cancers (Dotsch et al., 2015; Himmelfarb et al., 2004; Kloten et al., 2014; Mai et al., 2014; Rose et al., 2014).

Finally, we sought to identify autocrine/paracrine regulators of vascular cell function in a pro-atherosclerotic setting (Figure 3G). Using aorta expression profiles from an HMDP study where mice were genetically sensitized for atherosclerosis (Bennett et al., 2015), we asked whether the same approach could be applied to a complex vascular milieu of cells to uncover autocrine/paracrine factors. We observed PPBP as an enriched secreted factor with QENIE (Figure 3G), and GO analysis of *Ppbp* expression suggested a role for the protein in enhancing inflammatory processes (Figure 3H). Consistent with the pathway enrichment, mice injected with the protein showed elevated levels of aortic interleukin-1β (Figure 3I). We also observed similar trends in expression for tumor necrosis factor alpha and interferon gamma, which affected many additional tissues (data not shown), suggesting that the protein robustly promotes inflammatory cascades in an autocrine/paracrine and endocrine fashion. Despite a small size (~120 amino acids), the PPBP protein is proteolytically cleaved to produce several functionally distinct peptides (Ehlert et al., 1998; Holt et al., 1986), one of which has been found to be increased in patients with acute coronary disease (Ma and Liew, 2003; Smith et al., 2006). Although other studies have described distinct roles for these peptide products in various processes, we show that PPBP acts in an autocrine/paracrine manner to enhance aortic inflammation. Collectively, these data provide evidence that our generalized method can be applied to additional populations to uncover new regulators of tissue-tissue communication.

Identification of Lipocalin-5 as an Endocrine Regulator of Skeletal Muscle Metabolism

Since skeletal muscle is the most abundant organ in the body and is responsible for most fuel oxidation, we sought an endocrine factor that targets skeletal muscle to regulate metabolic processes and improve pathophysiologic metabolic status. Based on the pathway enrichment and high significance score of cross-organ analysis using the HF/HS panel shown in Figures 1 and 2, we chose to focus on the adipose-expressed protein, Lipocalin-5 (LCN5). Although little is known about the evolutionarily conserved function of LCN5, the protein belongs to a larger family of lipocalins that have been implicated in many diverse physiologic roles (Du et al., 2015; Flower et al., 2000; Schiefner and Skerra, 2015). Expression of *Lcn5* was approximately 3-fold higher in adipose tissue compared with others via qPCR (Figure 4A). Further, the BioGPS arrays used for tissue-specific expression filtering showed a much higher degree of expression in adipose tissue (Figure S2A). GO analysis showed highly significant enrichment for metabolic pathway regulation, specifically mitochondrial components in skeletal muscle (Figure 4B). As additional support for the metabolic relevance of the gene, we also observed a highly significant negative correlation among the 106 HMDP strains between body weight, various fat depot weights, and total fat mass percentage with adipose *Lcn5* expression (Figure 4C). Based on these observations, we hypothesized that LCN5 is an endocrine factor acting on skeletal muscle to regulate mitochondrial biogenesis and consequent oxidative capacity.

After identifying LCN5 as a potential adipose-derived regulator of skeletal muscle metabolism, we tested this connection in several models to assess mitochondrial function. To verify that signaling is mediated by LCN5 itself, we treated differentiated C2C12 myotubes, a commonly used model of skeletal muscle function, with LCN5 recombinant protein. LCN5 acted on C2C12 cells in a dose-dependent manner (Figure S6), and a dose of 1 μg/mL purified LCN5 protein was sufficient to induce robust expression of genes associated with both mitochondrial biogenesis and oxidation (Figure 4D). Consistent with changes in gene expression, LCN5 treatment enhanced the protein content of mitochondrial electron transport chain complexes (Figure 4E). To show that changes in gene expression and protein levels of oxidative machinery leads to an enhanced capacity of LCN5 to elevate skeletal muscle oxidation directly, myotubes treated with the same dose of protein were assessed for cellular respiration using a Seahorse system (Brown et al., 2007). Consistent with changes in gene expression, recombinant LCN5 significantly enhanced both basal (Figures 4F and 4G) and maximal respiratory capacity (Figures 4F and 4H) in myotubes. Although the differences under basal conditions appeared small (Figures 4F and 4G) relative to stimulated conditions, both remained significant across three independent experiments. To confirm that a direct physiologic mechanism persists whereby LCN5 derived from fat cells is capable of enhancing skeletal muscle oxidation, we performed experiments in which 3T3L1 adipocytes were infected with adeno-associated virus containing either GFP (AAV-GFP) or Lcn5 (AAV-LCN5) and co-cultured with three cell lines (Figures 4I–4K). AAV-LCN5 treatment lead to a ~10-fold increase in expression compared with GFP control (Figure S7). Consistent with observations above, two of the strongest genes induced by recombinant protein (*Sdhc* and *Atp5f1*) were also enhanced specifically when AAV-LCN5-infected adipocytes were cultured with myotubes (Figure 4I) and not liver (Figure 4J) or adipocytes (Figure 4K). These data show that LCN5 acts in a manner consistent with the inferred pathways to enhance mitochondrial respiratory activity in myotubes.

Overexpression of LCN5 in the Mouse Enhances Muscle Mitochondria Complex Function and Improves Glucose Metabolism

Our next aim was to evaluate the physiologic significance of elevated LCN5 levels in a mouse model of diet-induced insulin resistance. Mice administered an HF/HS diet for 6 weeks were injected with adenovirus encoding Lcn5 (Ad-LCN5) or control (Ad-GFP), where a majority of the overexpression was detected in liver and adipose tissue. One week following injection, mice were evaluated for various metabolic parameters. Although no difference in body weight was observed in this short time period between groups, the cohort that received Ad-LCN5 showed significantly enhanced metabolic parameters. Specifically, an approximate 2.2-fold increase in plasma levels (Figure S8) was sufficient to enhance glucose and insulin sensitivity (Figures 5A–5D). The effects of Ad-LCN5 in improving glucose regulation also persisted, albeit to a much lesser extent, under normal chow conditions (Figure S9). Consistent with the *in vitro* results, Ad-LCN5 significantly increased abundance of skeletal muscle insulin signaling components protein kinase B (Akt) and mammalian target of rapamycin (Figure 5E), as well as enhanced mitochondrial complex abundance (Figure 5F) in whole gastrocnemius muscle. To show that this physiologic circuit acts in a manner consistent with predictions, the same mice were interrogated for gene expression across relevant metabolic tissues. Here, we observed substantial skeletal muscle specificity for the action of LCN5 on both regulators of biogenesis (Figure 5G) and oxidation (Figure 5H). We also tested whether chronic expression of *Lcn5* could affect diet-induced obese phenotypes by using an AAV encoding LCN5 under the control of an adiponectin promoter. To increase the adipose tissue specificity of expression, this construct contains a 3′ microRNA122 binding motif, resulting in select degradation if expressed in the liver (O'Neill et al., 2014). Although the induction of overexpression was modest in these mice (~15% increase in plasma concentration), LCN5 expression slightly, but significantly, enhanced glucose and insulin tolerance (Figure S10). Unlike the short-term adenoviral study, long-term expression of LCN5 using AAV enhanced lean mass (Figure S10B). Further, these observations were consistent whether mice were administered the AAV either at the onset (Figures S10A–S10E) or following (Figures S10F–S10J) metabolic perturbation via HF/HS diet. Consistent with this notion, activation of Akt has been demonstrated to promote skeletal muscle hypertrophy (Lai et al., 2004). Understanding whether the Akt pathway is directly involved in LCN5-mediated lean mass growth would be of interest. We next utilized the GFP-tagged LCN5 from these mice to infer site of tissue action, where skeletal muscle showed the highest amount of GFP. It is worth noting that there were greater relative amounts of GFP in slow-twitch oxidative fiber (Soleus) compared with fast glycolytic (Plantaris), suggesting that LCN5 might preferentially bind oxidative fiber types (Figure S11). These observations illustrate the physiologic impacts of both acute and chronic overexpression of *Lcn5*.

Extension of LCN5/6 Functional Impact and Cross-Tissue Scoring from Mice to Humans

Initially, we sought to gauge the therapeutic relevance of these observations and test the application of LCN5 in human disease. The most conserved protein between species is another lipocalin family member, Lipocalin-6 (LCN6) (Hamil et al., 2003). To assess the functional impact of the LCN6 protein, primary human muscle cells harvested from healthy male donors were treated with recombinant human LCN6 protein (1 μg/mL). Treatment resulted in similar induction of the expression of master mitochondrial biogenesis and oxidation regulators (Figure 6A), and enhanced basal (Figure 6B) and maximal (Figure 6C) respiratory capacity was observed. These observations indicate that the functional impacts of mouse LCN5 can be recapitulated in a human system using the orthologous protein, LCN6.

Next, to gain an unbiased view of overlap between mouse and humans, we utilized a human dataset of RNA-seq from several tissues. These include visceral and subcutaneous adipose tissue, muscle, and liver from the Stockholm-Tartu Atherosclerosis Reverse Networks Engineering Task study (STARNET) (Franzen et al., 2016). We first asked if application of QENIE to human tissues showed concordance between mouse and human orthologous genes. In comparing the two datasets using Spearman correlation, we observed a significant positive overall correlation ($r = 0.121$, $p = 1.85 \times 10^{-23}$) between the S_{sec} from mice and humans from corresponding tissues (Figure S12).

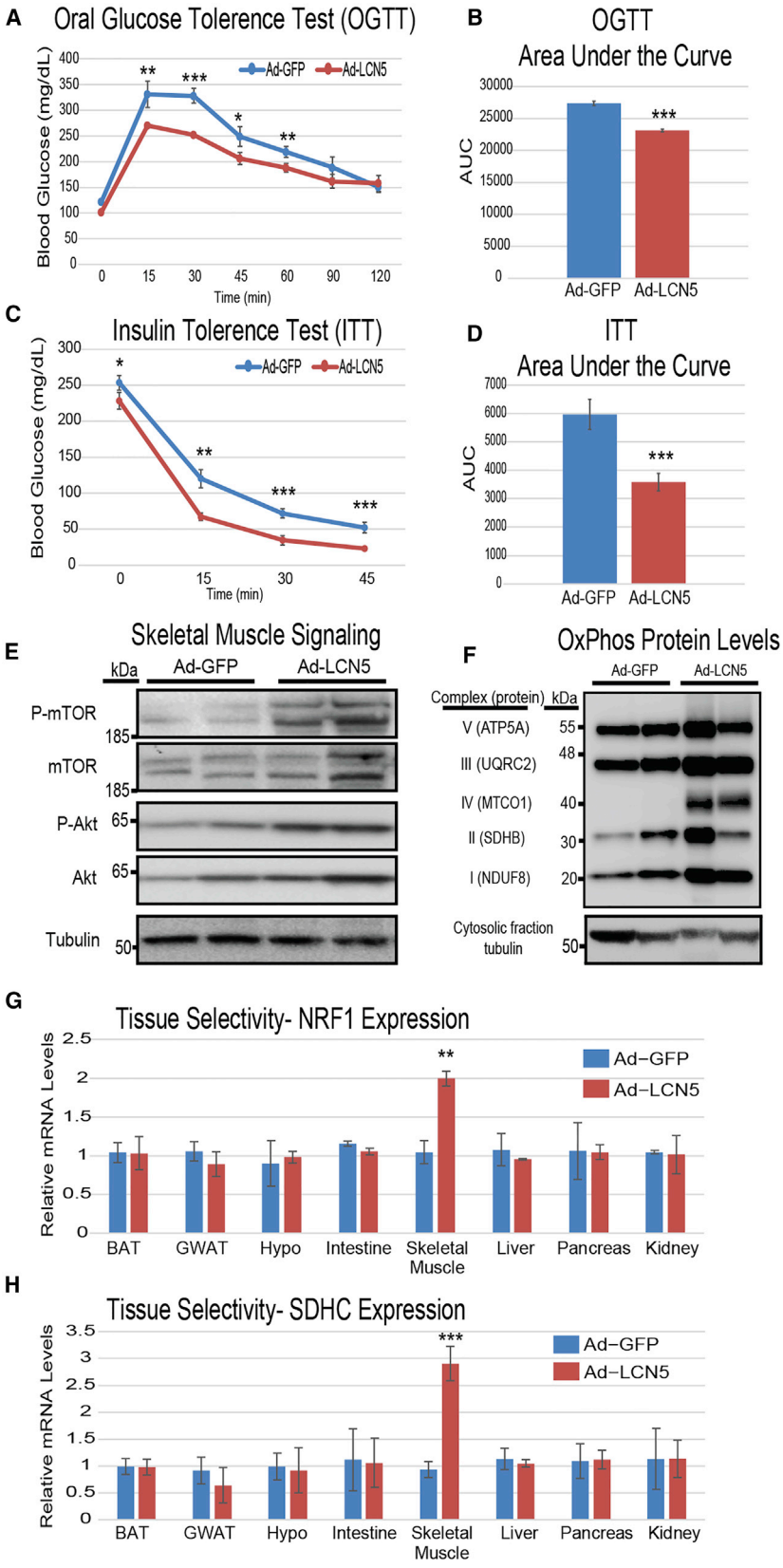

Figure 5. *Lcn5* Overexpression Reverses the Effects of Diet-Induced Metabolic Syndrome by Enhancing Skeletal Muscle Mitochondrial Abundance

(A–H) Mice fed an HF/HS diet for 6 weeks were administered either Ad-*GFP* or Ad-*Lcn5*, then evaluated for oral glucose tolerance (A and B), insulin tolerance (C and D), skeletal muscle insulin signaling cascades (E), or mitochondrial complex abundance (F). The same animals were subjected to qPCR analysis for predicted genes *Nrf1* (G) and *Sdhc* (H) across various tissues. n = 5 per group, each tolerance test was performed on a separate group of mice. All data presented as means ± SEM *p < 0.05, **p < 0.01, ***p < 0.001.

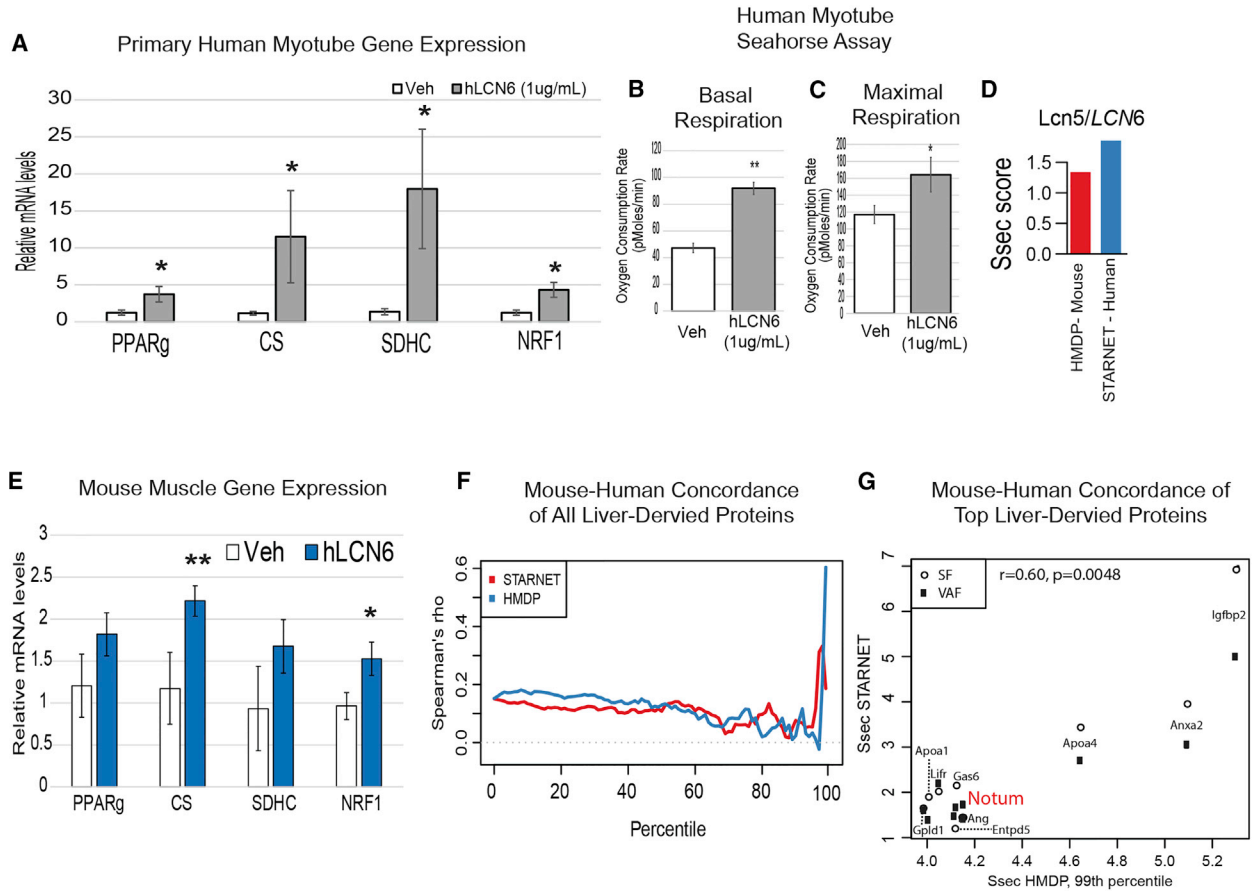

Figure 6. Concordance of Mouse and Human Data Using the QENIE Pipeline

As discussed in the text, *Lcn6* is the predicted functional ortholog of mouse *Lcn5*.

(A) Primary human myotubes were treated overnight with PBS (Veh) or LCN6 (1 μg/mL), and gene expression was evaluated using qPCR. n = 6.

(B and C) Primary human myotubes were treated for 30 hr with Veh or LCN6 (1 μg/mL) and then subjected to Seahorse bioanalyzer system, where significantly enhanced basal (B) and maximal (C) respiratory capacity was observed. n = 4 per group. All data presented as means ± SEM *p < 0.05, **p<0.01.

(D) S_{sec} scores for both mouse LCN5 (red) and human LCN6 in HMDP and STARNET, respectively.

(E) Gene expression from gastrocnemius in mice 8 hr after injection of PBS (Veh) or 0.1 μg/g body weight recombinant human LCN6. n = 6. **p<0.01.

(F) Spearman's rho correlation between S_{sec} of all mouse and human orthologous peptides (y axis) as a measure of S_{sec} score percentile within each dataset (x axis) originating from liver. Note the sharp increase in rho at the tail end of the percentile distribution.

(G) The top 1% of the HMDP genes from were correlated against their S_{sec} in STARNET from liver across either visceral (VAF, black squares) or subcutaneous (SF, open circles) fat, with NOTUM highlighted in red.

Also, in common with mouse LCN5, we found that LCN6 also scored highly and similarly in STARNET for visceral adipose to muscle tissue (Figure 6D), supporting experimental data (Figures 6A–6C). To provide additional evidence for the orthologous functions of LCN5 and LCN6, mice were injected with recombinant human LCN6, where we observed similar induction of skeletal muscle gene expression (Figure 6E). These data show human LCN6 as an ortholog for mouse LCN5 at both levels of regulation, as well as function, and illustrate that our generalized approach can be easily applied to human datasets.

Application of QENIE to Uncover *Notum* as a Liver-Derived Enhancer of White Adipose Beiging Gene Expression

In comparing the mouse and human populations, we next asked which inter-tissue circuits showed the strongest similarities between the two datasets. Since we assume that bona fide endocrine circuits will be found for a small fraction of genes in the tail end of cross-tissue significance distributions, we focused on the top subset of proteins for each axis. Therefore, individual genes were ranked from lowest-to-highest S_{sec} percentile within each dataset (x axis) and plotted against their Spearman's rho correlation between mouse and human orthologous gene scores (y axis) from liver to adipose tissue (Figure 6F). Within the liver-derived endocrine factors, we observed a striking concordance among orthologous gene S_{sec} scores at the top percentiles, where we expect to find proteins mediating inter-tissue communication (Figures 6F and 6G). Here, the top 1% of all HMDP S_{sec}-scored secreted proteins from liver showed significant positive correlation ($r = 0.6$, $p = 0.0048$) with adipose tissue S_{sec} in STARNET (Figure 6G).

Within this top percentile of genes, we found Notum pectinacetylesterase homolog (NOTUM), suggested to regulate a liver to white adipose tissue axis (Table S1; Figures 2E and 6F). Although NOTUM has been extensively studied and acts in part through inhibition of Wnt signaling, it has never been demonstrated to act on adipose tissue. The tissue distribution of *Notum* transcripts via qPCR and BioGPS shows that expression is highly restricted to liver (Figures 7A and S2B), and pathway enrichment analysis suggested that NOTUM enhances catabolic and brown adipose tissue-like machinery (Figure 7B). Consistent with this, we observed negative correlations between adipose *Notum* expression and fat mass traits across our panel of inbred strains (Figure 7C). Based on these data, we hypothesized that liver-derived NOTUM acts as a conserved enhancer of adipose tissue thermogenesis.

To experimentally test the hypothesis, we treated 3T3L1 adipocytes for the first 3 days of brown differentiation with vehicle or 200 ng/mL NOTUM, a protocol that has been previously used to test whether various pharmacologic agents could promote beiging of 3T3L1 adipocytes (Asano et al., 2014; Zhang et al., 2014). We observed increased expression of PGC1a and UCP1, markers of beiging, in cells treated with NOTUM (Figure 7D). Given that several other "beige" target genes, including iodothyronine deiodinase 2 (*Dio2*), and PR domain containing 16 (*Prdm16*) were below the detection limit of qPCR in 3T3L1 adipocytes, we adopted another *in vitro* model to test the hypothesis in which NOTUM promotes beige gene expression. Therefore, pre-BAT cells were differentiated into brown-like adipocytes, as described previously (Rodriguez-Cuenca et al., 2007; Villanueva et al., 2013), in the presence of vehicle or 200 mg/mL of NOTUM. Here, we also observed significantly enhanced gene expression of brown adipocyte markers (Figure 7E). Finally, we adopted a traditional culture model of browning, primary inguinal cultured cells. Following 4 days of treatment with recombinant NOTUM protein, we observed a marked induction of the same markers of browning (Figure 7F). Under these conditions, the average Ct values of browning genes were lower than those of 3T3L1 adipocytes (~24 versus 30), suggesting a more relevant physiologic setting to explore the impacts of the protein.

To validate the functional impact of NOTUM *in vivo*, mice were injected with adenoviral vectors containing GFP (Ad-GFP) or *Notum* (Ad-Notum). Nine days following injection, where circulating NOTUM levels increased ~2-fold (Figure S8), we observed significant increases in the same two beige markers in subcutaneous adipose, brown adipose, and, to a lesser extent, gonadal adipose tissue (Figures 7G and 7H). Here, a tissue-wide interrogation of *Ucp1* and *Pparg* also showed that the capacity of NOTUM to enhance these two genes is specific for fat cells, consistent with the prediction based on the QENIE method. Although the largest changes in *Ucp1* and *Pparg* transcription were observed in adipose tissue depots, expression was also altered in other tissues such as kidney and intestine. These observations suggest that Notum affects other organs when overexpressed for 9 days, either through direct action of the circulating protein or as a secondary response from the impact of adipose tissue. We also observed increased UCP1 protein expression in subcutaneous and brown fat pads, but not visceral (Figure 7I).

Next, we asked whether the impact of beige gene expression and protein levels was sufficient to enhance whole-body functional outcomes. Histological examination showed smaller size and less abundance of adipocytes within the Ad-Notum group (Figure 7J), with the most notable difference in the subcutaneous fat. To assess the physiologic significance of *Notum* overexpression, mice were subjected to a cold tolerance test. During an acute cold challenge, mice expressing Ad-*Notum* showed a markedly enhanced capacity to sustain body heat (Figure 7K). Next, to gain additional insight as to the impact of NOTUM on whole-body physiology mice were studied in metabolic chambers. Ad-*Notum* mice kept at 5°C showed increased oxygen consumption (Figure 7L) and produced more and carbon dioxide (Figure 7M), with no differences in food intake or respiratory exchange ratio (Figure S13) compared with controls. Although statistically significant respiratory differences were not observed at room temperature (despite a trend toward increases), all molecular phenotypes (Figure S13) persisted in the absence of a cold stress. Taken together, these data provide strong validation that NOTUM constitutes a novel physiologic mechanism in mice by which the liver can enhance thermogenesis in adipose tissue.

DISCUSSION

We present a framework for investigating endocrine circuits between tissues based on natural variation in gene expression populations of mice. The method requires global transcriptomic or proteomic data from the tissues of interest in a sufficient number of individuals to provide statistical power for the detection of correlation structure between the endocrine factor and its downstream effects in the target tissue. For this purpose, we have utilized a panel of approximately 100 inbred strains, the HMDP, maintained under defined environmental conditions. Our preliminary analysis of expression data from the STARNET population resource suggests that the method will be applicable to human populations as well. Future investigation of cross-tissue circuits in other human datasets, such as communication among inter-tissue signals in GTEX (GTEx Consortium, 2013), or identification of signaling between tumor and adjacent healthy tissue in TCGA, offer the potential for greater translation of these factors to human disease and physiology. Undoubtedly, due to environmental factors, age differences, inability to cleanly access relevant tissues, and lack of replications, the human data are expected to be much noisier than mouse data. The validity of the approach is supported by the fact that many of the predicted endocrine circuits are already known. Another key aspect of the method is to utilize pathway enrichment to define the likely molecular targets of the endocrine factors. In the case of the HMDP resource, we were also able to utilize previous clinical and physiologic data, which enabled us to formulate hypotheses regarding the targets of the putative endocrine factors. Finally, we have developed a straightforward pipeline to experimentally test the predictions of our bioinformatic analyses, involving expression of the endocrine factor for both *in vitro* and *in vivo* assessment of its impact. To demonstrate the utility of our approach for discovery, we report the physiologic impact of two novel endocrine factors, LCN5/6 and NOTUM, and *in vivo* experimental validation of three additional factors. Below, we

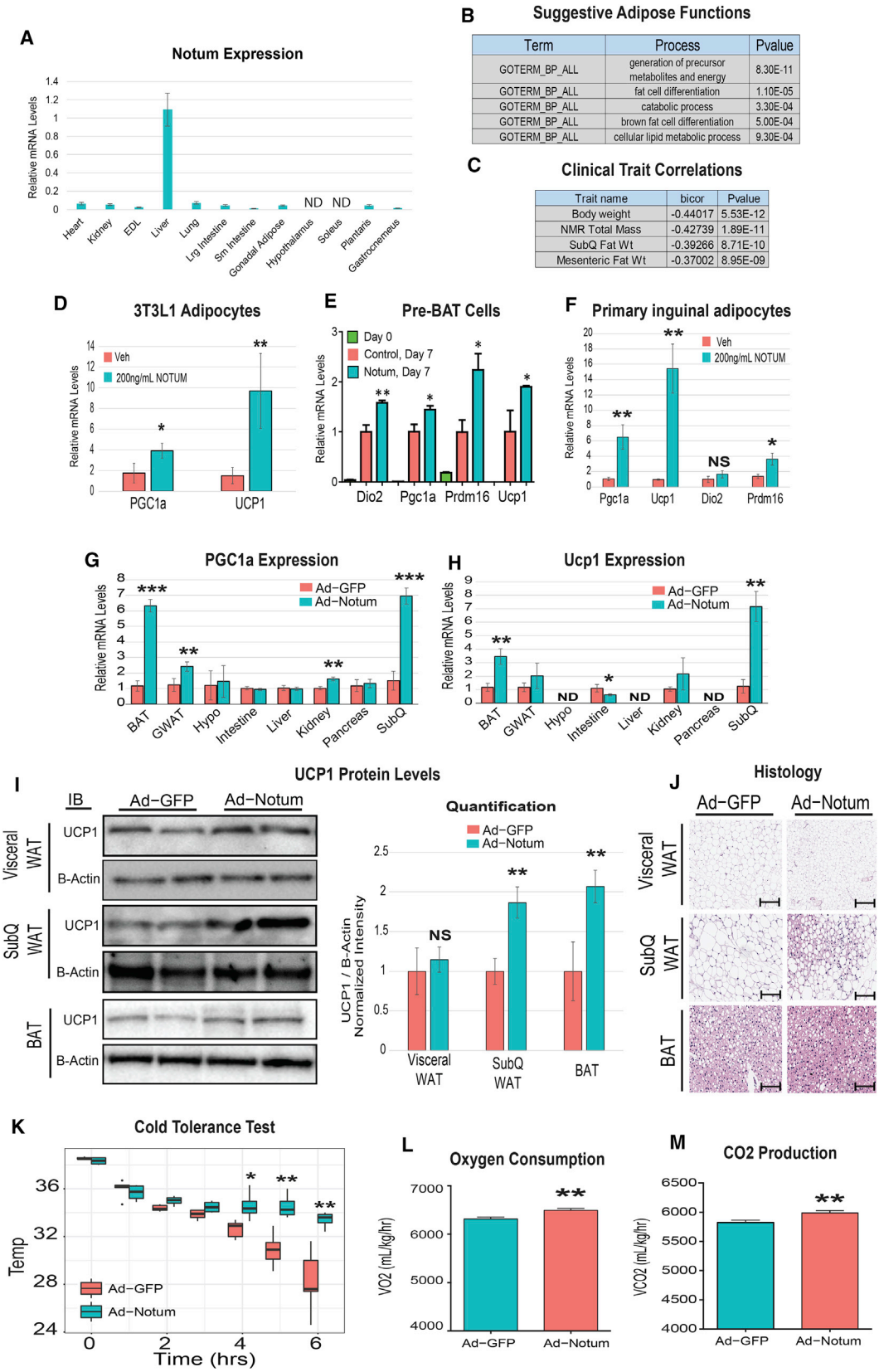

(legend on next page)

discuss some consideration relating to the future application of our method and the implications of our findings relating to LCN5/6, NOTUM and the other validated endocrine circuits.

Mouse LCN5 was first described as a small-molecular-weight protein secreted by the murine epididymis, where, unlike other closely conserved lipocalins, it did not show a strong affinity for binding spermatozoa (Hamil et al., 2003; Rankin et al., 1992b). It belongs to a larger family of proteins characterized by their ability to bind and carry small molecules via a conserved hydrophobic binding pocket in circulation (Flower et al., 2000; Schiefner and Skerra, 2015). LCN5 has been shown to bind *cis*- and *trans*-retinoic acid, but not retinol via application of labeled retinoic acid to DEAE ion-exchange chromatography (Rankin et al., 1992a). Although a specific factor in which LCN5 binds has yet to be described, the protein could potentially promote uptake of a factor involved in oxidation into muscle. Some preliminary experiments from our group indicate that the protein alone can enhance gene expression in cultured myotubes. Additional mechanistic studies will be required to narrow a receptor-mediated pathway. Prior to this study there has been no description of the regulation and role of *Lcn5* in adipose tissue. However, epididymal gene expression can be strongly induced by androgen receptor activation, a pathway that is suppressed by both castration (Lareyre et al., 1998) and forkhead box transcription factor 2 subclass A (Yu et al., 2006). Given the significant roles for forkhead box transcription factors and hormone signaling in impacting metabolic homeostasis, the mechanism of LCN5 could offer insight into how these components intertwine to mediate sex-specific differences in whole-body metabolism. Although the half-life of LCN5 *in vivo* is not known, the turnover of family member Lipocalin-2 is fairly rapid (10–20 min) (Axelsson et al., 1995), which has implications for the regulation and efficacy. Much less has been described with regard to the regulation and function of human LCN6, which was initially cloned based on cDNA sequence similarity to LCN5 and LCN8. The impact of LCN5 transcriptional components mediating mitochondrial abundance and function (Figures 4H and 4I) suggest a specific signaling axis, although we cannot exclude the possibility that other physiologic effects are so exclusive, requiring tissue-wide functional assays. The capacity of the protein to enhance whole-body glucose metabolism was markedly greater under HF/HS dietary conditions when compared with chow diet. Although we do not have a clear explanation for these observations, it is worth noting that QENIE predictions for LCN5 function were made using a mouse population fed an HF/HS diet (Parks et al., 2013, 2015). Specifically, evaluation of mice expressing LCN5 and LCN6 using metabolic cages or similar measurements under different dietary conditions will be informative to the physiologic consequence to protein action, thus guiding mechanism-based investigation. Moreover, while acute changes in LCN5 expression (adenovirus) did not alter body mass composition, chronic overexpression (through AAV) was sufficient to promote lean mass (Figure S10). A possible mechanism would be that cycles of acute LCN5-mediated sensitization of Akt signaling cascades (Figure 4E) occurred over a prolonged period, where elevated Akt is driving muscle proliferation. Consistent with this notion, activation of Akt has been demonstrated to promote skeletal muscle hypertrophy (Lai et al., 2004); however, proving the relationship to LCN5 function requires further exploration.

The NOTUM protein was first described in *Drosophila* as a secreted repressor of Wingless activity and a regulator of morphogenesis gradients (Giraldez et al., 2002). In human cells, NOTUM has been demonstrated to act as a hydrolase, releasing GPI-anchored proteins from the cell surface (Traister et al., 2008) and fine-tuning the Hedgehog pathway (Ayers et al., 2010, 2012). A recent study also showed that NOTUM can act as a carboxylesterase, removing palmitoleate from key members of the Wnt pathway and blunting signaling capacity (Kakugawa et al., 2015). Recently, a liver-specific deletion of *Notum* was reported. The authors did not observe ablation of Wnt/β-catenin signaling but did document changes in hepatic glucose output (Canal et al., 2016). Our study is the first to document effects of NOTUM on adipose tissue. The relatively rapid response (~9 days) of subcutaneous beiging highlights the efficacy of the protein and offers insight into potential mechanisms. Several acute physiologic conditions have been shown to enhance thermogenic features in subcutaneous fat, including modulating angiogenesis (Park et al., 2017) or increasing catecholamine signaling (Collins, 2011). It is also noteworthy that we observe slight, but significant, changes in kidney PGC1a following Notum overexpression. Both Wnt signaling (Logan and Nusse, 2004; Pulkkinen et al., 2008) and PGC1a (Lynch et al., 2017; Stadler et al., 2015) have been demonstrated to significantly affect kidney development and disease. Wnt signaling has been widely demonstrated to regulate adipose tissue function and differentiation and, recently, inhibition of Wnt has been linked to beiging of adipose tissue (Fulzele et al., 2017; Lo et al., 2016).

Figure 7. QENIE Uncovers *Notum* as a Liver-Derived Enhancer of Adipose Tissue Thermogenesis

(A) qPCR analysis of Lcn5 expression across indicated tissues in C57BL/6J mice. n = 6.

(B) Suggestive pathway enrichment using Database for Annotation, Visualization and Integrated Discovery output for top white adipose genes correlating with liver *Notum* expression.

(C) *Notum* liver expression in the HMDP shows negative correlations with body weight and fat mass.

(D) 3T3L1 adipocytes reached confluency then subjected to differentiation using a standard cocktail containing PBS (Veh) or 200 ng/mL NOTUM for 3 days. Following this treatment, medium was removed and protocol was carried out for 5 days, when RNA was extracted, reverse transcribed, and qPCR-investigated for gene expression (n = 6).

(E) pre-BAT cells were incubated with recombinant NOTUM throughout differentiation and qPCR-evaluated for similar beiging markers (n = 6).

(F) Primary inguinal adipocytes were isolated and cultured, followed by treatment with Veh or recombinant NOTUM protein for 4 days and analyzed for the same genes as in (E).

(G–J) Mice were injected with adenovirus containing cDNA sequence for GFP or *Notum*, then tissues were qPCR-probed for *Pgc1a* (G) and *Ucp1* (H) gene expression and adipose depots were immunoblotted for UCP1 protein (I) and subjected to histological examination (J).

(K) To assess physiologic parameters, Ad-*GFP* or Ad-*Notum* mice underwent cold tolerance tests (K), as well as metabolic chamber analysis at 5°C.

(L–M) ND, not detected (assessed by a raw qPCR Ct value above 30). All data presented as means ± SEM *p < 0.05, **p < 0.01, ***p < 0.001.

Our studies reveal novel potential endocrine functions for SMOC1, ITIH5, and PPBP based on changes in gene expression in pathways predicted using the QENIE method. Clearly, additional experiments are required to assess the physiologic impacts of these molecules. Our findings do, however, illustrate the broad potential applications of our approach to not only metabolism but also processes such as inflammation and growth regulation.

Limitations of Study

Our pipeline carries several caveats that should be considered. First, the process of identification eliminates secreted proteins that are ubiquitously expressed in many diverse cell types, but that could nonetheless still function as endocrine factors. Of note, several growth factor family members (fetal growth factors and insulin-like growth factors [Bottcher and Niehrs, 2005; Froesch et al., 1985; Jones and Clemmons, 1995; Nies et al., 2015]) and conserved family members based on sequence similarities to immune-acting peptides (interleukins and C1Q superfamily [Cunningham and De Souza, 1993; Harbuz et al., 1992; Pedersen and Febbraio, 2008; Seldin et al., 2012, 2014]) were consistently highly ranked, but were eliminated (Figures 2C–2G) after examination of tissue-specific expression. These proteins could of course be included in the analysis, but this would introduce doubt regarding the primary source of these proteins and therefore dilute subsequent interpretation based on enrichment of correlated gene expression in target tissues. In addition, the rate of bona fide interactions discovered using this method could be substantially influenced by the system used for screening (e.g., *in vitro* versus *in vivo*) and the genetic architecture and size of the populations. For example, long-range disequilibrium due to population structure among the HMDP could result in correlation between a locus controlling a secreted factor and the genetic regulation of genes elsewhere in the genome that are expressed in a target tissue. Also, one might imagine if a secreted protein and a gene in a target tissue are both affected by the same genetic locus, it could lead to false correlations and higher S_{sec} values. Although we cannot absolutely rule out all sources of confounders, the results from permutation testing (Figure 2; Table S1) suggest that these factors have no more than a minor impact on the results. This conclusion is further supported by the finding that the method reveals many known endocrine factors. Another important consideration is that organism-wide expression patterns due to physiologic status (such as global metabolic state) could bias cross-tissue scores by acting through latent variables. In a scenario where both expression of origin tissue gene and target tissue pathways are regulated by insulin, significant cross-tissue enrichment could be observed, not as a result of direct circuit of communication, but rather that both the gene and target pathways are conditioned on the impact of insulin. For this reason, it is essential to experimentally confirm mechanisms of putative secreted proteins, as illustrated for the five proteins described above. Investigation of the upstream physiologic factors that regulate expression of these secreted factors (beyond natural variation) would be especially informative as to their conserved physiologic roles. It is also worth noting that, while this pipeline identifies inter-tissue circuits based on expression in a single origin tissue, our screening process selects for proteins only sufficient to alter target tissue expression profiles where expression of the protein is not necessarily regulated by its physiologic source of production. Finally, the S_{sec} scores are based not only on the significance of correlations but also on the number of correlated genes. Hence, endocrine factors that affect pathways with feedback involving many cellular processes (e.g., altering global cellular metabolism) or that affect large gene expression programs will tend to dominate the S_{sec} score ranking. In contrast, endocrine factors that regulate fewer genes will be ranked lower, but might still serve important endocrine roles. An alternative strategy that would compute significance scores of peptides on groups of genes divided into individual pathways (e.g., immune system components) or co-correlated gene modules (Franzen et al., 2016) would also be a potential approach to target regulators of specific inter-tissue processes and perhaps enhance the resolution of detecting interactions.

In conclusion, we have developed a population-based approach for identifying novel communication axes between tissues and cell types using correlation structure. We have utilized a well-characterized and diverse population of mice, but our results suggest that other populations, including human cohorts, can be used. Endocrine functions have been identified for only a tiny fraction of secreted proteins, and our method provides a straightforward approach to expand our understanding. Clearly, such understanding may lead to novel therapeutic strategies. Our framework may be applicable to analyses of strong inter-tissue crosstalk beyond endocrine circuits, such as metabolite-mediated signals and microbiota-host interactions. We expect that as global proteomics data become available these will be particularly informative.

STAR★METHODS

Detailed methods are provided in the online version of this paper and include the following:

- KEY RESOURCES TABLE
- CONTACT FOR REAGENT AND RESOURCE SHARING
- EXPERIMENTAL MODELS AND SUBJECT DETAILS
  - Animals
  - Adeno-Associated Virus
  - Adenovirus
  - Cell Culture
  - Adipocyte Cell Culture
  - Primary Human Skeletal Muscle Cultures
- METHOD DETAILS
  - Coculture Experiments
  - Immunoblot Procedure and Analysis
  - Plasma Protein Measurements
  - Mitochondrial Preparation
  - Metabolic Cages
  - Cold Tolerance Test
  - Seahorse Biosystems
  - Reagents and Chemicals
  - RNA Extraction and Reverse Transcription
  - Quantitative PCR

SUPPLEMENTAL INFORMATION

Supplemental Information includes 13 figures and 1 table and can be found with this article online at https://doi.org/10.1016/j.cmet.2018.03.015.

ACKNOWLEDGMENTS

We thank Rosa Chen for help in preparing the manuscript. We also thank members of the Vallim-Tarling lab for providing experimental expertise. This work was supported by the following funding sources: NIH-T32HL007895 (to M.M.S.), NIH-T32HL69766 (to M.M.S.), NIH-HL28481 (to A.J.L.), NIH HL30568 (to A.J.L.), NIH-R00HL121172 (to M.C.), and the Fondation Leducq (*CADgenomics*: Understanding CAD Genes, 12CVD02) (to A.J.L. and J.L.M.B.).

AUTHOR CONTRIBUTIONS

M.M.S., G.M.R., P.R., K.C.K., L.V., Y.M., M.M., T.M.N.P., E.D.K., and R.G. performed the experiments. M.M.S., P.R., S.K., G.M.R., L.V., and D.M.S. analyzed raw data. S.M. and H.A.K. provided human muscle cells and expertise with respect to interpretation of human experiments. N.C., C.P., P.R., P.T., M.C., B.W.P., F.N., Y.H.-B., M.L., C.A.D., K.R., J.L.M.B. and A.J.L. reviewed the data and made substantial contributions to improving the studies. C.P., S.K., J.L.M.B., R.M.C., and A.J.L. provided statistical consult on permutation analyses. M.M.S. and A.J.L. wrote the manuscript, which was reviewed by all authors.

DECLARATION OF INTERESTS

The authors have no competing interests to declare.

Received: August 15, 2017
Revised: December 14, 2017
Accepted: March 24, 2018
Published: May 1, 2018

REFERENCES

Alvarez-Llamas, G., Szalowska, E., de Vries, M.P., Weening, D., Landman, K., Hoek, A., Wolffenbuttel, B.H., Roelofsen, H., and Vonk, R.J. (2007). Characterization of the human visceral adipose tissue secretome. Mol. Cell Proteomics *6*, 589–600.

Anveden, A., Sjoholm, K., Jacobson, P., Palsdottir, V., Walley, A.J., Froguel, P., Al-Daghri, N., McTernan, P.G., Mejhert, N., Arner, P., et al. (2012). ITIH-5 expression in human adipose tissue is increased in obesity. Obesity (Silver Spring) *20*, 708–714.

Asano, H., Kanamori, Y., Higurashi, S., Nara, T., Kato, K., Matsui, T., and Funaba, M. (2014). Induction of beige-like adipocytes in 3T3-L1 cells. J. Vet. Med. Sci. *76*, 57–64.

Ashburner, M., Ball, C.A., Blake, J.A., Botstein, D., Butler, H., Cherry, J.M., Davis, A.P., Dolinski, K., Dwight, S.S., Eppig, J.T., et al. (2000). Gene ontology: tool for the unification of biology. The Gene Ontology Consortium. Nat. Genet. *25*, 25–29.

Awwad, K., Hu, J., Shi, L., Mangels, N., Abdel Malik, R., Zippel, N., Fisslthaler, B., Eble, J.A., Pfeilschifter, J., Popp, R., et al. (2015). Role of secreted modular calcium-binding protein 1 (SMOC1) in transforming growth factor beta signalling and angiogenesis. Cardiovasc. Res. *106*, 284–294.

Axelsson, L., Bergenfeldt, M., and Ohlsson, K. (1995). Studies of the release and turnover of a human neutrophil lipocalin. Scand. J. Clin. Lab. Invest. *55*, 577–588.

Ayers, K.L., Gallet, A., Staccini-Lavenant, L., and Therond, P.P. (2010). The long-range activity of Hedgehog is regulated in the apical extracellular space by the glypican Dally and the hydrolase Notum. Dev. Cell *18*, 605–620.

Ayers, K.L., Mteirek, R., Cervantes, A., Lavenant-Staccini, L., Therond, P.P., and Gallet, A. (2012). Dally and Notum regulate the switch between low and high level Hedgehog pathway signalling. Development *139*, 3168–3179.

Belardelli, F. (1995). Role of interferons and other cytokines in the regulation of the immune response. APMIS *103*, 161–179.

Bennett, B.J., de Aguiar Vallim, T.Q., Wang, Z., Shih, D.M., Meng, Y., Gregory, J., Allayee, H., Lee, R., Graham, M., Crooke, R., et al. (2013). Trimethylamine-N-oxide, a metabolite associated with atherosclerosis, exhibits complex genetic and dietary regulation. Cell Metab. *17*, 49–60.

Bennett, B.J., Davis, R.C., Civelek, M., Orozco, L., Wu, J., Qi, H., Pan, C., Packard, R.R., Eskin, E., Yan, M., et al. (2015). Genetic architecture of atherosclerosis in mice: a systems genetics analysis of common inbred strains. PLoS Genet. *11*, e1005711.

Bottcher, R.T., and Niehrs, C. (2005). Fibroblast growth factor signaling during early vertebrate development. Endocr. Rev. *26*, 63–77.

Brown, L.D., Rodney, G.G., Hernandez-Ochoa, E., Ward, C.W., and Schneider, M.F. (2007). Ca2+ sparks and T tubule reorganization in dedifferentiating adult mouse skeletal muscle fibers. Am. J. Physiol. Cell Physiol. *292*, C1156–C1166.

Canal, F., Charawi, S., Grimber, G., Houbron, C., Drouet, V., Colnot, S., Terris, B., Cavard, C., and Perret, C. (2016). Generation of mice with hepatocyte-specific conditional deletion of Notum. PLoS One *11*, e0150997.

Civelek, M., and Lusis, A.J. (2014). Systems genetics approaches to understand complex traits. Nat. Rev. Genet. *15*, 34–48.

Collins, S. (2011). Beta-adrenoceptor signaling networks in adipocytes for recruiting stored fat and energy expenditure. Front. Endocrinol. (Lausanne) *2*, 102.

Cunningham, E.T., Jr., and De Souza, E.B. (1993). Interleukin 1 receptors in the brain and endocrine tissues. Immunol. Today *14*, 171–176.

Dotsch, M.M., Kloten, V., Schlensog, M., Heide, T., Braunschweig, T., Veeck, J., Petersen, I., Knuchel, R., and Dahl, E. (2015). Low expression of ITIH5 in adenocarcinoma of the lung is associated with unfavorable patients' outcome. Epigenetics *10*, 903–912.

Du, J., Yuan, Z., Ma, Z., Song, J., Xie, X., and Chen, Y. (2014). KEGG-PATH: Kyoto encyclopedia of genes and genomes-based pathway analysis using a path analysis model. Mol. Biosyst. *10*, 2441–2447.

Du, Z.P., Wu, B.L., Wu, X., Lin, X.H., Qiu, X.Y., Zhan, X.F., Wang, S.H., Shen, J.H., Zheng, C.P., Wu, Z.Y., et al. (2015). A systematic analysis of human lipocalin family and its expression in esophageal carcinoma. Sci. Rep. *5*, 12010.

Ehlert, J.E., Gerdes, J., Flad, H.D., and Brandt, E. (1998). Novel C-terminally truncated isoforms of the CXC chemokine beta-thromboglobulin and their impact on neutrophil functions. J. Immunol. *161*, 4975–4982.

Elmquist, J.K., Maratos-Flier, E., Saper, C.B., and Flier, J.S. (1998). Unraveling the central nervous system pathways underlying responses to leptin. Nat. Neurosci. *1*, 445–450.

Farooqi, I.S., and O'Rahilly, S. (2009). Leptin: a pivotal regulator of human energy homeostasis. Am. J. Clin. Nutr. *89*, 980S–984S.

Flower, D.R., North, A.C., and Sansom, C.E. (2000). The lipocalin protein family: structural and sequence overview. Biochim. Biophys. Acta. *1482*, 9–24.

Franzen, O., Ermel, R., Cohain, A., Akers, N.K., Di Narzo, A., Talukdar, H.A., Foroughi-Asl, H., Giambartolomei, C., Fullard, J.F., Sukhavasi, K., et al. (2016). Cardiometabolic risk loci share downstream cis- and trans-gene regulation across tissues and diseases. Science *353*, 827–830.

Friedman, J.M., and Halaas, J.L. (1998). Leptin and the regulation of body weight in mammals. Nature *395*, 763–770.

Froesch, E.R., Schmid, C., Schwander, J., and Zapf, J. (1985). Actions of insulin-like growth factors. Annu. Rev. Physiol. *47*, 443–467.

Fulzele, K., Lai, F., Dedic, C., Saini, V., Uda, Y., Shi, C., Tuck, P., Aronson, J.L., Liu, X., Spatz, J.M., et al. (2017). Osteocyte-secreted Wnt signaling inhibitor sclerostin contributes to beige adipogenesis in peripheral fat depots. J. Bone Miner. Res. *32*, 373–384.

Gehlenborg, N., O'Donoghue, S.I., Baliga, N.S., Goesmann, A., Hibbs, M.A., Kitano, H., Kohlbacher, O., Neuweger, H., Schneider, R., Tenenbaum, D., et al. (2010). Visualization of omics data for systems biology. Nat. Methods *7*, S56–S68.

Gene Ontology Consortium (2015). Gene ontology consortium: going forward. Nucleic Acids Res. *43*, D1049–D1056.

Giraldez, A.J., Copley, R.R., and Cohen, S.M. (2002). HSPG modification by the secreted enzyme Notum shapes the Wingless morphogen gradient. Dev. Cell *2*, 667–676.

Graham, T.E., Yang, Q., Bluher, M., Hammarstedt, A., Ciaraldi, T.P., Henry, R.R., Wason, C.J., Oberbach, A., Jansson, P.A., Smith, U., et al. (2006). Retinol-binding protein 4 and insulin resistance in lean, obese, and diabetic subjects. N. Engl. J. Med. *354*, 2552–2563.

GTEx Consortium (2013). The genotype-tissue expression (GTEx) project. Nat. Genet. *45*, 580–585.

Hamil, K.G., Liu, Q., Sivashanmugam, P., Anbalagan, M., Yenugu, S., Soundararajan, R., Grossman, G., Rao, A.J., Birse, C.E., Ruben, S.M., et al. (2003). LCN6, a novel human epididymal lipocalin. Reprod. Biol. Endocrinol. *1*, 112.

Harbuz, M.S., Stephanou, A., Sarlis, N., and Lightman, S.L. (1992). The effects of recombinant human interleukin (IL)-1 alpha, IL-1 beta or IL-6 on hypothalamo-pituitary-adrenal axis activation. J. Endocrinol. *133*, 349–355.

Hasin-Brumshtein, Y., Khan, A.H., Hormozdiari, F., Pan, C., Parks, B.W., Petyuk, V.A., Piehowski, P.D., Brummer, A., Pellegrini, M., Xiao, X., et al. (2016). Hypothalamic transcriptomes of 99 mouse strains reveal trans eQTL hotspots, splicing QTLs and novel non-coding genes. Elife *5*, https://doi.org/10.7554/eLife.15614.

Hathout, Y. (2007). Approaches to the study of the cell secretome. Expert Rev. Proteomics *4*, 239–248.

Himmelfarb, M., Klopocki, E., Grube, S., Staub, E., Klaman, I., Hinzmann, B., Kristiansen, G., Rosenthal, A., Durst, M., and Dahl, E. (2004). ITIH5, a novel member of the inter-alpha-trypsin inhibitor heavy chain family is downregulated in breast cancer. Cancer Lett. *204*, 69–77.

Holt, J.C., Harris, M.E., Holt, A.M., Lange, E., Henschen, A., and Niewiarowski, S. (1986). Characterization of human platelet basic protein, a precursor form of low-affinity platelet factor 4 and beta-thromboglobulin. Biochemistry *25*, 1988–1996.

Huang, D.W., Sherman, B.T., Tan, Q., Collins, J.R., Alvord, W.G., Roayaei, J., Stephens, R., Baseler, M.W., Lane, H.C., and Lempicki, R.A. (2007). The DAVID Gene Functional Classification Tool: a novel biological module-centric algorithm to functionally analyze large gene lists. Genome Biol. *8*, R183.

Jones, J.I., and Clemmons, D.R. (1995). Insulin-like growth factors and their binding proteins: biological actions. Endocr. Rev. *16*, 3–34.

Joyce, A.R., and Palsson, B.O. (2006). The model organism as a system: integrating 'omics' data sets. Nat. Rev. Mol. Cell Biol. *7*, 198–210.

Kadowaki, T., Yamauchi, T., Kubota, N., Hara, K., Ueki, K., and Tobe, K. (2006). Adiponectin and adiponectin receptors in insulin resistance, diabetes, and the metabolic syndrome. J. Clin. Invest. *116*, 1784–1792.

Kakugawa, S., Langton, P.F., Zebisch, M., Howell, S.A., Chang, T.H., Liu, Y., Feizi, T., Bineva, G., O'Reilly, N., Snijders, A.P., et al. (2015). Notum deacylates Wnt proteins to suppress signalling activity. Nature *519*, 187–192.

Katz-Jaffe, M.G., McReynolds, S., Gardner, D.K., and Schoolcraft, W.B. (2009). The role of proteomics in defining the human embryonic secretome. Mol. Hum. Reprod. *15*, 271–277.

Keller, M.P., Choi, Y., Wang, P., Davis, D.B., Rabaglia, M.E., Oler, A.T., Stapleton, D.S., Argmann, C., Schueler, K.L., Edwards, S., et al. (2008). A gene expression network model of type 2 diabetes links cell cycle regulation in islets with diabetes susceptibility. Genome Res. *18*, 706–716.

Kershaw, E.E., and Flier, J.S. (2004). Adipose tissue as an endocrine organ. J. Clin. Endocrinol. Metab. *89*, 2548–2556.

Kersten, S., Mandard, S., Tan, N.S., Escher, P., Metzger, D., Chambon, P., Gonzalez, F.J., Desvergne, B., and Wahli, W. (2000). Characterization of the fasting-induced adipose factor FIAF, a novel peroxisome proliferator-activated receptor target gene. J. Biol. Chem. *275*, 28488–28493.

Klok, M.D., Jakobsdottir, S., and Drent, M.L. (2007). The role of leptin and ghrelin in the regulation of food intake and body weight in humans: a review. Obes. Rev. *8*, 21–34.

Kloten, V., Rose, M., Kaspar, S., von Stillfried, S., Knuchel, R., and Dahl, E. (2014). Epigenetic inactivation of the novel candidate tumor suppressor gene ITIH5 in colon cancer predicts unfavorable overall survival in the CpG island methylator phenotype. Epigenetics *9*, 1290–1301.

Kusminski, C.M., McTernan, P.G., and Kumar, S. (2005). Role of resistin in obesity, insulin resistance and type II diabetes. Clin. Sci. (Lond.) *109*, 243–256.

Kussmann, M., Raymond, F., and Affolter, M. (2006). OMICS-driven biomarker discovery in nutrition and health. J. Biotechnol. *124*, 758–787.

Lai, K.M., Gonzalez, M., Poueymirou, W.T., Kline, W.O., Na, E., Zlotchenko, E., Stitt, T.N., Economides, A.N., Yancopoulos, G.D., and Glass, D.J. (2004). Conditional activation of akt in adult skeletal muscle induces rapid hypertrophy. Mol. Cell Biol. *24*, 9295–9304.

Langfelder, P., and Horvath, S. (2008). WGCNA: an R package for weighted correlation network analysis. BMC Bioinformatics *9*, 559.

Langfelder, P., and Horvath, S. (2012). Fast R functions for robust correlations and hierarchical clustering. J. Stat. Softw. *46*.

Lareyre, J.J., Zheng, W.L., Zhao, G.Q., Kasper, S., Newcomer, M.E., Matusik, R.J., Ong, D.E., and Orgebin-Crist, M.C. (1998). Molecular cloning and hormonal regulation of a murine epididymal retinoic acid-binding protein messenger ribonucleic acid. Endocrinology *139*, 2971–2981.

Lawlor, K., Nazarian, A., Lacomis, L., Tempst, P., and Villanueva, J. (2009). Pathway-based biomarker search by high-throughput proteomics profiling of secretomes. J. Proteome Res. *8*, 1489–1503.

Lazarczyk, M.A., Lazarczyk, M., and Grzela, T. (2003). Ghrelin: a recently discovered gut-brain peptide (review). Int. J. Mol. Med. *12*, 279–287.

Leinonen, R., Nardone, F., Zhu, W., and Apweiler, R. (2006). UniSave: the UniProtKB sequence/annotation version database. Bioinformatics *22*, 1284–1285.

Lindskog, C. (2015). The potential clinical impact of the tissue-based map of the human proteome. Expert Rev. Proteomics *12*, 213–215.

Lo, K.A., Ng, P.Y., Kabiri, Z., Virshup, D., and Sun, L. (2016). Wnt inhibition enhances browning of mouse primary white adipocytes. Adipocyte *5*, 224–231.

Logan, C.Y., and Nusse, R. (2004). The Wnt signaling pathway in development and disease. Annu. Rev. Cell Dev. Biol. *20*, 781–810.

Long, Q., Argmann, C., Houten, S.M., Huang, T., Peng, S., Zhao, Y., Tu, Z.; GTEx Consortium, and Zhu, J. (2016). Inter-tissue coexpression network analysis reveals DPP4 as an important gene in heart to blood communication. Genome Med. *8*, 15.

Lynch, M.R., Tran, M.T., and Parikh, S.M. (2017). PGC1alpha in the kidney. Am. J. Physiol. Renal Physiol. *314*, F1–F8.

Ma, J., and Liew, C.C. (2003). Gene profiling identifies secreted protein transcripts from peripheral blood cells in coronary artery disease. J. Mol. Cell Cardiol. *35*, 993–998.

Mai, C., Zhao, J.J., Tang, X.F., Wang, W., Pan, K., Pan, Q.Z., Zhang, X.F., Jiang, S.S., Zhao, B.W., Li, Y.F., et al. (2014). Decreased ITIH5 expression is associated with poor prognosis in primary gastric cancer. Med. Oncol. *31*, 53.

Makridakis, M., and Vlahou, A. (2010). Secretome proteomics for discovery of cancer biomarkers. J. Proteomics *73*, 2291–2305.

Margetic, S., Gazzola, C., Pegg, G.G., and Hill, R.A. (2002). Leptin: a review of its peripheral actions and interactions. Int. J. Obes. Relat. Metab. Disord. *26*, 1407–1433.

Martin, J., Midgley, A., Meran, S., Woods, E., Bowen, T., Phillips, A.O., and Steadman, R. (2016). Tumor necrosis factor-stimulated gene 6 (TSG-6)-mediated interactions with the inter-alpha-inhibitor heavy chain 5 facilitate tumor

growth factor beta1 (TGFbeta1)-dependent fibroblast to myofibroblast differentiation. J. Biol. Chem. *291*, 13789–13801.

Miller, M.B., and Bassler, B.L. (2001). Quorum sensing in bacteria. Annu. Rev. Microbiol. *55*, 165–199.

Mosmann, T.R., and Coffman, R.L. (1989). TH1 and TH2 cells: different patterns of lymphokine secretion lead to different functional properties. Annu. Rev. Immunol. *7*, 145–173.

Mosquera, G., Giraldo, M.C., Khang, C.H., Coughlan, S., and Valent, B. (2009). Interaction transcriptome analysis identifies *Magnaporthe oryzae* BAS1-4 as biotrophy-associated secreted proteins in rice blast disease. Plant Cell *21*, 1273–1290.

Nian, M., Lee, P., Khaper, N., and Liu, P. (2004). Inflammatory cytokines and postmyocardial infarction remodeling. Circ. Res. *94*, 1543–1553.

Nielsen, H., Engelbrecht, J., Brunak, S., and von Heijne, G. (1997). Identification of prokaryotic and eukaryotic signal peptides and prediction of their cleavage sites. Protein Eng. *10*, 1–6.

Nies, V.J., Sancar, G., Liu, W., van Zutphen, T., Struik, D., Yu, R.T., Atkins, A.R., Evans, R.M., Jonker, J.W., and Downes, M.R. (2015). Fibroblast growth factor signaling in metabolic regulation. Front. Endocrinol. (Lausanne) *6*, 193.

O'Gorman, T.W. (2002). An adaptive test of significance for a subset of regression coefficients. Stat. Med. *21*, 3527–3542.

O'Neill, S.M., Hinkle, C., Chen, S.J., Sandhu, A., Hovhannisyan, R., Stephan, S., Lagor, W.R., Ahima, R.S., Johnston, J.C., and Reilly, M.P. (2014). Targeting adipose tissue via systemic gene therapy. Gene Ther. *21*, 653–661.

Ogata, H., Goto, S., Sato, K., Fujibuchi, W., Bono, H., and Kanehisa, M. (1999). KEGG: Kyoto encyclopedia of genes and genomes. Nucleic Acids Res. *27*, 29–34.

Okada, I., Hamanoue, H., Terada, K., Tohma, T., Megarbane, A., Chouery, E., Abou-Ghoch, J., Jalkh, N., Cogulu, O., Ozkinay, F., et al. (2011). SMOC1 is essential for ocular and limb development in humans and mice. Am. J. Hum. Genet. *88*, 30–41.

Park, J., Kim, M., Sun, K., An, Y.A., Gu, X., and Scherer, P.E. (2017). VEGF-a-expressing adipose tissue shows rapid beiging and enhanced survival after transplantation and confers IL-4-independent metabolic improvements. Diabetes *66*, 1479–1490.

Parks, B.W., Nam, E., Org, E., Kostem, E., Norheim, F., Hui, S.T., Pan, C., Civelek, M., Rau, C.D., Bennett, B.J., et al. (2013). Genetic control of obesity and gut microbiota composition in response to high-fat, high-sucrose diet in mice. Cell Metab. *17*, 141–152.

Parks, B.W., Sallam, T., Mehrabian, M., Psychogios, N., Hui, S.T., Norheim, F., Castellani, L.W., Rau, C.D., Pan, C., Phun, J., et al. (2015). Genetic architecture of insulin resistance in the mouse. Cell Metab. *21*, 334–347.

Pedersen, B.K., and Febbraio, M.A. (2008). Muscle as an endocrine organ: focus on muscle-derived interleukin-6. Physiol. Rev. *88*, 1379–1406.

Petricoin, E.F., and Liotta, L.A. (2004). SELDI-TOF-based serum proteomic pattern diagnostics for early detection of cancer. Curr. Opin. Biotechnol. *15*, 24–30.

Pierson, E., GTEx Consortium, Koller, D., Battle, A., Mostafavi, S., Ardlie, K.G., Getz, G., Wright, F.A., Kellis, M., Volpi, S., et al. (2015). Sharing and specificity of co-expression networks across 35 human tissues. PLoS Comput. Biol. *11*, e1004220.

Price, A.L., Helgason, A., Thorleifsson, G., McCarroll, S.A., Kong, A., and Stefansson, K. (2011). Single-tissue and cross-tissue heritability of gene expression via identity-by-descent in related or unrelated individuals. PLoS Genet. *7*, e1001317.

Pulkkinen, K., Murugan, S., and Vainio, S. (2008). Wnt signaling in kidney development and disease. Organogenesis *4*, 55–59.

Rainger, J., van Beusekom, E., Ramsay, J.K., McKie, L., Al-Gazali, L., Pallotta, R., Saponari, A., Branney, P., Fisher, M., Morrison, H., et al. (2011). Loss of the BMP antagonist, SMOC-1, causes Ophthalmo-acromelic (Waardenburg Anophthalmia) syndrome in humans and mice. PLoS Genet. *7*, e1002114.

Rankin, T.L., Ong, D.E., and Orgebin-Crist, M.C. (1992a). The 18-kDa mouse epididymal protein (MEP 10) binds retinoic acid. Biol. Reprod. *46*, 767–771.

Rankin, T.L., Tsuruta, K.J., Holland, M.K., Griswold, M.D., and Orgebin-Crist, M.C. (1992b). Isolation, immunolocalization, and sperm-association of three proteins of 18, 25, and 29 kilodaltons secreted by the mouse epididymis. Biol. Reprod. *46*, 747–766.

Rocchi, M., Covone, A., Romeo, G., Faraonio, R., and Colantuoni, V. (1989). Regional mapping of RBP4 to 10q23→q24 and RBP1 to 3q21→q22 in man. Somat. Cell Mol. Genet. *15*, 185–190.

Rodriguez-Cuenca, S., Monjo, M., Frontera, M., Gianotti, M., Proenza, A.M., and Roca, P. (2007). Sex steroid receptor expression profile in brown adipose tissue. Effects of hormonal status. Cell Physiol. Biochem. *20*, 877–886.

Rose, M., Gaisa, N.T., Antony, P., Fiedler, D., Heidenreich, A., Otto, W., Denzinger, S., Bertz, S., Hartmann, A., Karl, A., et al. (2014). Epigenetic inactivation of ITIH5 promotes bladder cancer progression and predicts early relapse of pT1 high-grade urothelial tumours. Carcinogenesis *35*, 727–736.

Salomon, F., Cuneo, R.C., Hesp, R., and Sonksen, P.H. (1989). The effects of treatment with recombinant human growth hormone on body composition and metabolism in adults with growth hormone deficiency. N. Engl. J. Med. *321*, 1797–1803.

Scherer, P.E., Williams, S., Fogliano, M., Baldini, G., and Lodish, H.F. (1995). A novel serum protein similar to C1q, produced exclusively in adipocytes. J. Biol. Chem. *270*, 26746–26749.

Schiefner, A., and Skerra, A. (2015). The menagerie of human lipocalins: a natural protein scaffold for molecular recognition of physiological compounds. Acc. Chem. Res. *48*, 976–985.

Schwartz, M.W., Seeley, R.J., Campfield, L.A., Burn, P., and Baskin, D.G. (1996). Identification of targets of leptin action in rat hypothalamus. J. Clin. Invest. *98*, 1101–1106.

Seldin, M.M., Peterson, J.M., Byerly, M.S., Wei, Z., and Wong, G.W. (2012). Myonectin (CTRP15), a novel myokine that links skeletal muscle to systemic lipid homeostasis. J. Biol. Chem. *287*, 11968–11980.

Seldin, M.M., Lei, X., Tan, S.Y., Stanson, K.P., Wei, Z., and Wong, G.W. (2013). Skeletal muscle-derived myonectin activates the mammalian target of rapamycin (mTOR) pathway to suppress autophagy in liver. J. Biol. Chem. *288*, 36073–36082.

Seldin, M.M., Tan, S.Y., and Wong, G.W. (2014). Metabolic function of the CTRP family of hormones. Rev. Endocr. Metab. Disord. *15*, 111–123.

Sherman, B.T., Huang da, W., Tan, Q., Guo, Y., Bour, S., Liu, D., Stephens, R., Baseler, M.W., Lane, H.C., and Lempicki, R.A. (2007). DAVID Knowledgebase: a gene-centered database integrating heterogeneous gene annotation resources to facilitate high-throughput gene functional analysis. BMC Bioinformatics *8*, 426.

Skrobuk, P., von Kraemer, S., Semenova, M.M., Zitting, A., and Koistinen, H.A. (2012). Acute exposure to resveratrol inhibits AMPK activity in human skeletal muscle cells. Diabetologia *55*, 3051–3060.

Smith, C., Damas, J.K., Otterdal, K., Oie, E., Sandberg, W.J., Yndestad, A., Waehre, T., Scholz, H., Endresen, K., Olofsson, P.S., et al. (2006). Increased levels of neutrophil-activating peptide-2 in acute coronary syndromes: possible role of platelet-mediated vascular inflammation. J. Am. Coll. Cardiol. *48*, 1591–1599.

Stadler, K., Goldberg, I.J., and Susztak, K. (2015). The evolving understanding of the contribution of lipid metabolism to diabetic kidney disease. Curr. Diab. Rep. *15*, 40.

Steppan, C.M., Bailey, S.T., Bhat, S., Brown, E.J., Banerjee, R.R., Wright, C.M., Patel, H.R., Ahima, R.S., and Lazar, M.A. (2001). The hormone resistin links obesity to diabetes. Nature *409*, 307–312.

Su, A.I., Cooke, M.P., Ching, K.A., Hakak, Y., Walker, J.R., Wiltshire, T., Orth, A.P., Vega, R.G., Sapinoso, L.M., Moqrich, A., et al. (2002). Large-scale analysis of the human and mouse transcriptomes. Proc. Natl. Acad. Sci. U. S. A. *99*, 4465–4470.

Tedgui, A., and Mallat, Z. (2006). Cytokines in atherosclerosis: pathogenic and regulatory pathways. Physiol. Rev. *86*, 515–581.

Thomou, T., Mori, M.A., Dreyfuss, J.M., Konishi, M., Sakaguchi, M., Wolfrum, C., Rao, T.N., Winnay, J.N., Garcia-Martin, R., Grinspoon, S.K., et al. (2017).

Adipose-derived circulating miRNAs regulate gene expression in other tissues. Nature *542*, 450–455.

Traister, A., Shi, W., and Filmus, J. (2008). Mammalian Notum induces the release of glypicans and other GPI-anchored proteins from the cell surface. Biochem. J. *410*, 503–511.

Trujillo, M.E., and Scherer, P.E. (2005). Adiponectin – journey from an adipocyte secretory protein to biomarker of the metabolic syndrome. J. Intern. Med. *257*, 167–175.

Uhlen, M., Oksvold, P., Fagerberg, L., Lundberg, E., Jonasson, K., Forsberg, M., Zwahlen, M., Kampf, C., Wester, K., Hober, S., et al. (2010). Towards a knowledge-based human protein atlas. Nat. Biotechnol. *28*, 1248–1250.

UniProt Consortium (2015). UniProt: a hub for protein information. Nucleic Acids Res. *43*, D204–D212.

Villanueva, C.J., Vergnes, L., Wang, J., Drew, B.G., Hong, C., Tu, Y., Hu, Y., Peng, X., Xu, F., Saez, E., et al. (2013). Adipose subtype-selective recruitment of TLE3 or Prdm16 by PPARgamma specifies lipid storage versus thermogenic gene programs. Cell Metab. *17*, 423–435.

Williams, M.J. (1993). J. J. R. Macleod: the co-discoverer of insulin. Proc. R. Coll. Physicians Edinb. *23*, 1–125.

Wozniak, S.E., Gee, L.L., Wachtel, M.S., and Frezza, E.E. (2009). Adipose tissue: the new endocrine organ? A review article. Dig. Dis. Sci. *54*, 1847–1856.

Wu, C., Orozco, C., Boyer, J., Leglise, M., Goodale, J., Batalov, S., Hodge, C.L., Haase, J., Janes, J., Huss, J.W., 3rd, et al. (2009). BioGPS: an extensible and customizable portal for querying and organizing gene annotation resources. Genome Biol. *10*, R130.

Yoshida, K., Shimizugawa, T., Ono, M., and Furukawa, H. (2002). Angiopoietin-like protein 4 is a potent hyperlipidemia-inducing factor in mice and inhibitor of lipoprotein lipase. J. Lipid Res. *43*, 1770–1772.

Yu, X., Suzuki, K., Wang, Y., Gupta, A., Jin, R., Orgebin-Crist, M.C., and Matusik, R. (2006). The role of forkhead box A2 to restrict androgen-regulated gene expression of lipocalin 5 in the mouse epididymis. Mol. Endocrinol. *20*, 2418–2431.

Zhang, Y., Li, R., Meng, Y., Li, S., Donelan, W., Zhao, Y., Qi, L., Zhang, M., Wang, X., Cui, T., et al. (2014). Irisin stimulates browning of white adipocytes through mitogen-activated protein kinase p38 MAP kinase and ERK MAP kinase signaling. Diabetes *63*, 514–525.

STAR★METHODS

KEY RESOURCES TABLE

REAGENT or RESOURCE	SOURCE	IDENTIFIER
Antibodies		
Polyclonal LCN5	myBioSource	MBS2027564
rabbit monoclonal GFP	cell signaling	Cat# 2956S, RRID:AB_1196615
rabbit polyclonal NOTUM	Abcam	ab106448, RRID:AB_10864231
rabbit polyclonal α-tubulin	Cell Signaling	2144, RRID:AB_2210548
mouse anti-Noq7	Abcam	ab11083, RRID:AB_297734
Total OxPhos complex cocktail	Abcam	Cat# ab110413, RRID:AB_2629281
rabbit UCP1 polyclonal	Abcam	ab10983, RRID:AB_2241462
Bacterial and Virus Strains		
AAV8.hAdp.LCN5.miR122.SV40	Upenn	N/A
AAV8.hAdp.GFP.miR122.SV40	Upenn	N/A
Adeno-GFP	This Paper	N/A
Adeno-LCN5	This Paper	N/A
Adeno-NOTUM	This Paper	N/A
Chemicals, Peptides, and Recombinant Proteins		
Mouse LCN5	Mybiosource	MBS1006340
Human Notum	Origene	TP309331
Mouse ITIH5	Mybiosource	MBS1377888
Human SMOC1	Origene	TP304083
Human LCN6	Origene	TP309389
Mouse PPBP	Lifespan Biosystems	LS-G12044
Deposited Data		
HF/HS Array tissues	GEO	GEO: GSE64770
HF/HS Hypothalamus	GEO	GEO: GSE79551
Chow aorta	GEO	GEO: GSE38120
Chow heart	GEO	GEO: GSE77263
Chow adipose	GEO	GEO: GSE42890
Chow liver	GEO	GEO: GSE16780
Uniprot annotations for secreted proteins	www.uniprot.org/	location:"Secreted [SL-0243]" type:component) AND organism:"Mus musculus (Mouse) [10090]
BioGPS arrays to investigate tissue specificity	http://biogps.org/#goto=welcome	GeneAtlas GNF1M, gcrma
HF/HS preprocessed tissues	Github	https://github.com/marcus-seldin/QENIE
Experimental Models: Cell Lines		
Mouse C2C12 Myotubes	ATCC	CRL-1772
Human Primary Muscle Biopsies	This Paper	NA
3T3L1 Adipocytes	ATCC	CL-173
Pre-BAT cells	This paper	NA
Oligonucleotides		
Listed in STAR Methods		
Software and Algorithms		
Software: WGCNA package used for cross-tissue correlations	https://cran.r-project.org/	WGCNA
Software: Reshape2 package for data preprocessing	https://cran.r-project.org/	Reshape2

(*Continued on next page*)

Continued

REAGENT or RESOURCE	SOURCE	IDENTIFIER
Algorithm: bicorAndPvalue function from WGCNA package	WGCNA	bicorAndPvalue()
Software: R software environment for analyses	https://www.r-project.org/	R Studo
Repository for R script and analysis	Github	https://github.com/marcus-seldin/QENIE

CONTACT FOR REAGENT AND RESOURCE SHARING

Further information and requests for resources and reagents should be directed to and will be fulfilled by the Lead Contact, Jake Lusis – jlusis@mednet.ucla.edu.

EXPERIMENTAL MODELS AND SUBJECT DETAILS

Animals

All animal experiments were approved by the University of California Los Angeles (UCLA) Animal Care and Use Committee, in accordance with Public Health Service guidelines. C57BL/6J mice were purchased from the Jackson Laboratory. Beginning at 6 weeks of age, mice were fed a standard High-fat/High Sucrose diet (35% kcal fat, Research diets cat # D12266B). Mice were administered AAV via intraperitoneal injection at a titer of approximately 1e12 per mouse. Oral glucose tolerance tests were performed following an overnight fast. Mice were gavaged with 10 μL/gram body weight of a 10% (w/v) solution of glucose in PBS. Insulin tolerance tests were performed after a 4 hr fast, whereby animals administered 1U/kg body weight human recombinant insulin protein (Sigma). The cohort of mice testing LCN5 expression was administered a HF/HS diet prior to receiving adenovirus, while all other cohorts were fed a standard chow diet. For the recombinant protein injections, shown in Figure 3, mice were fasted overnight, then injected with 0.15 μg/gram body weight recombinant protein in PBS. Tissus were harvested for gene expression 6 hr following injection.

Adeno-Associated Virus

Mouse lipocalin-5 cDNA or GFP was cloned into an AAV expression plasmid purchased from the University of Pennsylvania Gene Therapy program vector core (AAV8.hAdp.GFP.miR122.SV40) driven under an adiponectin promoter. The plasmid was used to synthesize AAV which was carried out at the University of Pennsylvania Gene Therapy program vector core.

Adenovirus

Recombinant adenovirus was generated using the AdEasy system as previously described (Bennett et al., 2013). Briefly, linearized shuttle vector containing full-length mouse cDNA for *Notum* and *Lcn5* were transformed into *E. coli* BJ5183AD cells containing the adenoviral backbone plasmid pAdEasy-1 for homologous recombination. Positive recombinants were linearized and transfected into HEK293AD cells for virus packaging and propagation. Adenoviruses expressing the candidate gene were purified by CsCl banding and stored at −80°C until use. For adenoviral infection, 7-week-old male C57BL/6J mice were injected with adenoviral construct (~2.5×10^9 PFUs diluted in 0.2 mL saline) Intraperitoneally. After overnight fasting, mice were sacrificed 9 days post injection, tissues were extracted, the expression gene expression was assessed by RT-PCR. The control group consisted of mice injected with adenoviral construct expressing the GFP gene.

Cell Culture

C2C12 mouse myocytes were cultured as previously described (Seldin et al., 2012, 2013). In brief, myocytes were maintained below 60% confluency in high glucose (4.5 g/L) Debulcos Modified Eagles Medium (DMEM, Life Technologies) supplemented with 20% FBS (Altanta Biologicals), 100U/mL penicillin, 100 μg/mL streptomycin, 1 mmol/L sodium pyruvate and 4 mmol/L L-Glutamine. For differentiation into myotubes, cells were grown to >95% confluency and serum starved (DMEM containing 2% Horse Serum (Life Technologies) and lacking sodium pyruvate) for a period of 6-8 days. Differentiation of myotubes was confirmed morphologically by formation of multinucleated fibers. Transfections for introduction of exogenous DNA into cells were performed using Lipofectamine 2000 (Life Technologies) in accordance with the recommended protocol. For experiments involving concentrated media, cells transfected with indicated vectors were incubated in *Opti-MEM* Reduced Serum Media (Life Technologies) for 48 hr to allow sufficient amounts of protein to be secreted. Media was then harvested and concentrated using 10,000 molecular weight cut-off Centrifugal Filter Units (Millipore) as described in the product protocol.

Adipocyte Cell Culture

3T3L1 cells were maintained in below 60% confluency in high glucose (4.5 g/L) Debulcos Modified Eagles Medium (DMEM, Life Technologies) supplemented with 20% FBS (Atlanta Biologicals), 100 U/mL penicillin, 100 μg/mL streptomycin, 1 mmol/L sodium pyruvate and 4mmol/L L-Glutamine. Protocol for differentiation was carried out as previously described when cells

reached >95% confluency (Asano et al., 2014; Zhang et al., 2014). The mouse brown preadipocyte cell line (pre-BAT) were isolated from the stromal vascular fraction of mouse interscapular brown adipose tissues and immortalized by infecting with retrovirus vector expressing the SV40 T antigen and was cultured as previously described (Asano et al., 2014; Zhang et al., 2014). The pre-BAT cells were grown in DMEM (high glucose) supplemented with 10% fetal calf serum and 100 U/ml of both penicillin and streptomycin (growth media). For differentiation experiments. The pre-BAT cells were plated in 6-well plate at 1 × 10^6 cells per well. Three days after plating (day 0), when the cells reached nearly 100% confluency, the cells were treated with an induction media containing growth media supplemented with 5 μg/mL insulin, 1 nM 3,3',5-Triiodo-L-thyronine (T3), 125 μM indomethacin, 2 μg/mL dexamethasone, 0.5 mM 3-Isobutyl-1-methylxanthine, and 0.5 μM Rosiglitazone for 48 hr (day 0 to day 2). After 48 hr, the cells were treated with a maintenance media containing the growth media supplemented with 5 μg/mL insulin, 1 nM 3,3',5-Triiodo-L-thyronine (T3), and 0.5 μM Rosiglitazone, with a media change every 2-3 days until day 7 when RNA was isolated for gene expression analysis. For the NOTUM treatment group, 200 ng/mL of human recombinant NOTUM (Origene) were added to the induction media and the cells were treated with NOTUM from day 0 to day 2 for 48 hr. RNA samples were also collected from cells at day 0 as a baseline control.

Primary Human Skeletal Muscle Cultures

Primary human muscle cells were isolated and cultured as previously described (Skrobuk et al., 2012). In general, experiments were performed from 5-9 passages. Myocyte cells were growth in DMEM/F-12 media containing 25 mM glucose, GlutaMAX (Life Technologies), 20% FBS and antibiotic/antimycotic (Life Technologies) at low confluency. Differentiation treatments began when cells reached 80% confluency, where media was changed to DMEM/F-12 containing GlutaMAX (Life Technologies antibiotic/antimycotic (Life Technologies), 5 mM glucose and 2% FBS. Differentiation was carried out 5-7 days and confirmed by the formations of multinucleated muscle fibers. All treatments were carried out in the media used for differentiation.

METHOD DETAILS

Coculture Experiments

Each cell line was cultured under conditions as described above. Experiments were carried out in a trasnwell system (corning # 07-200-170). 3T3L1 adipocytes were plated into the culture insert and allowed to achieve confluency. Cells were then treated with AAV ($1E10^{10}$ per mL) for 24 hr. Cells were then washed and differentiated for 8 days (listed above). Following differentiation, adipocytes inserts were added to each respective cell line for 24 hr.

Immunoblot Procedure and Analysis

Cells and tissues were lysed in Whole Cell Extraction buffer (WCE) containing 62.5 mM Tris-HCl (pH 6.8), 2% (wt/v) Sodium dodecyl sulfate, and 10% glycerol. Samples were then heated and diluted 1:5 in water and protein content measured using a BCA protein assay kit (Pierce). Total protein concentration was normalized to 3 μg/uL and samples were then denatured in 4x LDS loading buffer (Life Technologies) with 10x reducing agent (Life Technologies) at 99°C for 20 min. Samples were then loaded at 10 μL/well into 4%-12% Bis-Tris gels (Invitrogen) and separated out at 130 volts for 2 hr. Protein was then transferred to PVDF membranes (Immobilon) for 1.5 hr at 35 volts. Following transfer, membranes were washed with TBST, and then blocked in 5% skim milk (Gibco) in TBST for 1 hr at room temperature. Membranes were then placed in primary antibodies (1:2000) on a shaker overnight at 4°C. Primary antibodies were used as follows rabbit polyclonal LCN5 (myBioSource # MBS2027564, 1:1000), rabbit monoclonal GFP (cell signaling # 2956S), rabbit polyclonal NOTUM (abcam # ab106448, 1:1000), rabbit polyclonal α-tubulin (Cell Signaling #2144, 1:2500), mouse anti-Noq7 (abcam #11083, 1:2000), Total OxPhos complex cocktail (abcam, # ab110413, 1:2000), rabbit UCP1 polyclonal (abcam # ab10983, 1:1000). The following day, membranes were washed 3X in TBST then placed in secondary antibodies (1:2000) for 1 hr at room temperature. Blots were then washed 3X in TBST and placed Amersham ECL detection solution (GE health sciences). Blots were imaged using IMAGER and bands were quantified using ImageJ Software.

Plasma Protein Measurements

Quantification of plasma proteins shown in Figure S8 were performed using immunoblot analysis (above) using equal volumes of recombinant protein vs plasma. While size differences appear between the bands indicated when comparing the two sample types, we confirmed these observations using multiple antibodies targeting different regions of the proteins.

Mitochondrial Preparation

Mitochondria lysate was prepared from either skeletal muscle or C2C12 myotubes using Fisher isolation kit (cat # 89874) according to manufacturer recommendations. For whole tissue, muscle was first trypsin digested then subjected to isolation procedure. Lysate was normalized to total cytosolic protein content then subjected to immunoblot procedure.

Metabolic Cages

Indirect calorimetry was performed using a Columbus Instruments Comprehensive Lab Animal Monitoring System. Animals were placed individually in chambers for 8 hr at cold temperature (5°C) with 12-hr light/dark cycles. Animals had free access to food and water. Oxygen (VO2) and carbon dioxide (CO2) respiratory measurements were made in 20-min intervals after an overnight acclimation period.

Cold Tolerance Test

To assess cold tolerance, C57BL/6J mice were placed in 4 degrees and monitored for body temperature using a rodent rectal temperature probe (World Precision Instruments) every hour for a period of 6 hr.

Seahorse Biosystems

Real-time measurement of oxygen consumption rate (OCR) in cells was carried out using the XF24 Extracellular Flux Analyzer (Agilent). To directly assess mitochondrial metabolism, OCR measurements were made before and after the sequential injection of 0.4 μM oligomycin (ATP synthase inhibitor, which allows determination of ATP-linked respiration), 1.5 μM FCCP (an uncoupler, which allows determination of maximal mitochondrial respiratory capacity), and 2 μM rotenone/myxothiazol (inhibitors of complex I/III of the electron transport chain, which allows determination of non-mitochondrial respiration). OCR was normalized per protein content using a bradford assay.

Reagents and Chemicals

HIS-tagged mecombinant mouse Lipocalin-5 produced in HEK293 cells was purchased from creative biomart. mouse ITIH5 protein purified from HEK 293 was purchased from MyBioSource. Recombinant NOTUM (human), Lipocalin-6 (human) and SMOC1 (human) and purchased from Origene. Recombinant PPBP (mouse) was purchased from Lifespan Biosystems. The protein purity was verified as >90% by Coomassie stain following SDS-PAGE. Treatment of cells with recombinant protein was performed overnight for qPCR analysis or 30 hr for Seahorse assay and protein quantification.

RNA Extraction and Reverse Transcription

Cells or tissue were homogenized in Qiazol (Qiagen) and RNA extraction was carried out as recommended. Samples were suspended in 0.5 mL Qiazol each then 100 μL chloroform was added. After vortexing, phase separation was achieved with centrifugation at 13k rpm for 15 min. The aqueous layer was then transferred to 1 mL isopropanol, vortexed then centrifuged again. The remaining pellets were washed in 70% ethanol in water then air dried following centrifugation for 10 min. Purified RNA was then suspended in 30 μL of water and assessed for purity and concentration using a Nanodrop ND-100 Spectophotometer. Two ug of total RNA per sample was reverse transcribed using a High-Capacity cDNA reverse transcription kit (Applied Biosystems) with random primers. Reverse-transcribed cDNA was then diluted in water for qPCR analysis.

Quantitative PCR

Quantitative PCR was carried out using a Kappa SYBR Fast qPCR kit as recommended by the manufacturer. Samples were ran on a LightCycler 480 II (Roche) and analyzed using the Roche LightCycler 1.5.0 Software. All qPCR targets were normalized to geometric mean of RPL13a and PPIA expression and quantified using the delta Ct method. All qPCR primer sequences were obtained from PrimerBank (http://pga.mgh.harvard.edu/primerbank). All Sequences to qPCR primers are listed below:

Species	Gene	Sequence 5' - > 3'
mouse	SIRT1- F	GCTGACGACTTCGACGAC
mouse	SIRT1 - R	TCGGTCAACAGGAGGTTGTCT
mouse	NRF2 - F	CTTTAGTCAGCGACAGAAGGAC
mouse	NRF2 - R	AGGCATCTTGTTTGGGAATGTG
mouse	Foxo1 - F	AAGGATAAGGGCGACAGCAA
mouse	Foxo1 -R	TCTTGCCCAGACTGGAGAGAT
mouse	Rpl13 - F	CTGTGAAGGCATCAACATTTCTG
mouse	Rpl13 - R	GACCACCATCCGCTTTTTCTT
mouse	Sdhc - F	GCTGCGTTCTTGCTGAGACA
mouse	Sdhc - R	ATCTCCTCCTTAGCTGTGGTT
mouse	PPIA - F	GAGCTGTTTGCAGACAAAGTTC
mouse	PPIA - R	CCCTGGCACATGAATCCTGG
mouse	CS - F	GGACAATTTTCCAACCAATCTGC
mouse	CS - R	AGTCAATGGCTCCGATACTGC
mouse	Ppargc1a - F	TATGGAGTGACATAGAGTGTGCT
mouse	Ppargc1a - R	GTCGCTACACCACTTCAATCC
mouse	Atp5f1 - F	AGTTCCTTTACCCTAAGACTGGT
mouse	Atp5f1 - R	TTCATGCTCGACTGCTTTACTT

(*Continued on next page*)

Continued

Species	Gene	Sequence 5' - > 3'
mouse	UCP1 - F	CGATGTCCATGTACACCAAGGA
mouse	UCP1 - R	TCGCAGAAAAGAAGCCACAA
mouse	LCN5 - F	CTCCAAGATGGGTGCATACGG
mouse	LCN5 - R	CCTCATTGTAATAGGTGGTGGTC
mouse	Cpt1a - F	CTCCGCCTGAGCCATGAAG
mouse	Cpt1a - R	CACCAGTGATGATGCCATTCT
mouse	Il1b - F	GCAACTGTTCCTGAACTCAACT
mouse	Il1b - R	ATCTTTTGGGGTCCGTCAACT
mouse	Tgfb1 - F	CTCCCGTGGCTTCTAGTGC
mouse	Tgfb1 - R	GCCTTAGTTTGGACAGGATCTG
human	PPARg - F	GGGATCAGCTCCGTGGATCT
human	PPARg - R	TGCACTTTGGTACTCTTGAAGTT
human	RPL13a - F	GCCATCGTGGCTAAACAGGTA
human	RPL13a - F	GTTGGTGTTCATCCGCTTGC
human	Cs - F	TGCTTCCTCCACGAATTTGAAA
human	CS - R	CCACCATACATCATGTCCACAG
human	PPIA - F	CCCACCGTGTTCTTCGACATT
human	PPIA - R	GGACCCGTATGCTTTAGGATGA
human	sdhc - F	CTGTTGCTGAGACACGTTGGT
human	sdhc - R	ACAGAGGACGGTTTGAACCTA
human	NRF1 -F	AGGAACACGGAGTGACCCAA
human	NRF1 - R	TATGCTCGGTGTAAGTAGCCA

QUANTIFICATION AND STATISTICAL ANALYSES

Statistical Analysis

All computational procedures were carried out using R statistical software. Correlations and associated p values were calculated with the biweight midcorrelation, which is robust to outliers and associated pvalue (Langfelder and Horvath, 2008, 2012). Single comparisons between two groups were performed using two-tailed Student's t tests with 95% confidence intervals. Comparisons involving multiple time points were assessed using a two-way ANOVA with Tukeys posthoc tests. Permutations of target tissue redistributions were carried out as described in Figure S2. Values were considered significant at $p < 0.05$. All data are presented as means ± SE.

Cross-Tissue Correlations and Optimization of Informatics Resources

Cross tissue biweight midcorrelation coefficients and corresponding pvalues were calculated using the R package WGCNA (Langfelder and Horvath, 2008, 2012). To retrieve and overlay annotated secreted proteins, we used the list deposited in the Universal Protein resource (UniProt) as ''secreted'' localization annotations [SL-0243] for overlapping HUGO symbol in Mus musculus (Mouse) [10090].

DATA AND SOFTWARE AVAILABILITY

Github

As referenced in the text, the R script used to perform the pipeline, data pretreatment, sample datasets, and example of qq-plots are available at https://github.com/marcus-seldin/QENIE.

Data Pretreatment

Mouse expression arrays for the original HF/HS HMDP studies were performed on a Affymetrix HT_MG-430A. The accession number for arrays is GEO: GSE64770

Our pipeline begins with gene expression arrays for liver and adipose tissue, where each gene is represented as an averaged value across probes and strains used in the study. These aggregate matrices are also provided in this repository. The arrays consisted of ~22,400 probes which were aggregated to averages for each gene (12,242). The expression values for each mouse were also averaged to reflect a single value per gene per strain (106). Therefore, each liver and adipose tissue expression matrix consists of 12,242 genes among 106 unique HMDP strains.

Datasets Used

The raw datasets used in this study (In addition to GSE64770) are available using the following GEO accessions: chow aorta, GEO: GSE38120; chow heart, GEO: GSE77263; chow liver, GEO: GSE16780; chow adipose, GEO: GSE42890; and HF/HS - hypothalamus, GEO: GSE79551. All other data are directly available on the Github.

Optimization of Ranking Lists for Pathway Enrichment

In an effort to provide optimal pathway enrichment using the target tissue correlation coefficents conditioned on each origin tissue secreted protein, we systematically screened these lists and assessed pvalues of GO biologic pathways. Here, we took all suggestive pathway lists for the top-ranked peptides within adipose, liver, and muscle (targeting all others) and assessed DAVID output for the top 100, 200, 500, 1000 or 2000 target tissue genes ranked by positive or negative bicor or p value. The top 3 GO biologic pathways showed the lowest average p values (Benjamani) using the list of 500 target tissue genes, ranked from highest-to-lowest bicor. It is worth noting that this generally conditions our approach to pathways positively enhanced by the peptide. Alternatively, using the ranking system of lowest-to-highest bicor could potentially condition for pathways suppressed by origin tissue peptides or using the p value to infer "general processes engaged." Examples of such are presented in Figure 3.

Cell Metabolism, Volume *27*

Supplemental Information

A Strategy for Discovery of Endocrine Interactions with Application to Whole-Body Metabolism

Marcus M. Seldin, Simon Koplev, Prashant Rajbhandari, Laurent Vergnes, Gregory M. Rosenberg, Yonghong Meng, Calvin Pan, Thuy M.N. Phuong, Raffi Gharakhanian, Nam Che, Selina Mäkinen, Diana M. Shih, Mete Civelek, Brian W. Parks, Eric D. Kim, Frode Norheim, Karthickeyan Chella Krishnan, Yehudit Hasin-Brumshtein, Margarete Mehrabian, Markku Laakso, Christian A. Drevon, Heikki A. Koistinen, Peter Tontonoz, Karen Reue, Rita M. Cantor, Johan L.M. Björkegren, and Aldons J. Lusis

Supplemental Materials:
Supplemental Figure Tables and Legends

SUPPLEMENTAL TABLE 1: Ssec and pvalue of permutation score for each top-ranked peptide, related to Figure 2

SUPPL FIG 1 – PERMUTATION TESTING AND OVERVIEW FIGURE

SUPPL FIG 2 – BIOGPS ARRAYS USED TO INFER TISSUE SPECIFICITY

SUPPL FIG 3 – SEX DIFFERENCES AMONG SSEC SCORES

SUPPL FIG 4 – ALTERNATIVE STRATEGIES TO CROSS-TISSUE CORRELATIONS

SUPPL FIG 5 – QQPLOTS FOR ENRICHMENT OF SECRETED FACTORS

SUPPL FIG 6 - LCN5 DOSE-DEPENDENT TREATMENT

SUPPL FIG 7 – LCN5 MRNA QUANTIFICATION IN COCULTURED MYOTUBES

SUPPL FIG 8 – PLASMA ADENO PROTEIN MEASUREMENTS

SUPPL FIG 9 – ADENO-LCN5 MICE ON NORMAL CHOW DIET ITT AND GTT

SUPPL FIG 10 – AAV-LCN5 COHORT EXPREIMENTS

SUPPL FIG 11 – TISSUE-WIDE GFP BLOTS TO ASSESS LCN5 TARGETS

SUPPL FIG 12 – CONCORDANCE OF SSEC BETWEEN HMDP AND STARTNET

SUPPL FIG 13 – NOTUM POOLED EXPERIMENT METABOLIC CAGE MEASUREMENTS

SUPPLEMENTARY MATERIAL

SUPPLEMENTARY FIGURE LEGENDS

SUPPL FIG 1 – PERMUTATION TESTING AND OVERVIEW FIGURE, related to Figure 2: An overview2 of the S_{sec} calculation is outlined starting with expression arrays from 2 tissues. In addition, we not the permutation tests with a green arrow on the right. Here, the observed S_{sec} score is tested against datasets with permuted target tissue strain expression. An example for the permutation for the top-ranked adipose-to-muscle gene is shown.

SUPPL FIG 2 – BIOGPS ARRAYS USED TO INFER TISSUE SPECIFICITY, related to Figure 4A and Figure 7A: BioGPS array data showing the tissue-wide expression of Lcn5 (**A**) and Notum (**B**).

SUPPL FIG 3 – SEX DIFFERENCES AMONG SSEC SCORES, related to Figure 2: For adipose and liver HMDP expression, S_{sec} was performed on sex and tissue-specific circuits. Plotted are the correlations between sexes of the relative S_{sec} ranking for all secreted proteins (**A, B**) or the 50 highest-ranked (**C, D**). We note very strong concordance of correlation with all genes, but significantly less when focusing on the top 50, which are inferred to represent the strongest axes of communication.

SUPPL FIG 4 – ALTERNATIVE STRATEGIES TO CROSS-TISSUE CORRELATIONS, related to Figure 1 and Figure 2: For the two cross-tissue circuits explored in detail, we are plotting the correlations of ranking for each protein derived from either S_{sec} or various pvalue cut-offs. Adipose-to-muscle is shown on top and liver-to-adipose on bottom. Since the correlations are particularly strong and, therefore, many genes overlap, a density count was included. The density count reflects the number of genes within a given spatial region to allow color representation overlapping values. We observe highly significant similarities amongst the

various ranking strategies for cross-tissue correlation, as evident by the indicated correlation coefficents and pvalues.

SUPPL FIG 5 – QQPLOTS FOR ENRICHMENT OF SECRETED FACTORS, related to Figure 1: For each cross-tissue axis in **Fig 2**, qqplots were generated by comparing cross-tissue S_{sec} scores for secreted proteins (y-axis) vs genes coding for non-secreted proteins (x-axis). Script used to generate QQ-Plots is also provided in the Github. To show this relationship, the sum of -ln(pvalue) was determined for all non-secreted factors, which when correlated against themselves on a scatterplot, producing the red line of perfect correlation. Next, secreted factors values were superimposed, where the y-axis position determined by the sum of -ln(pvalue) across target tissue transcripts and x-axis value were matched for bins of percentile based on the relative rank of correlation, corresponding to rankings between secreted and non-secreted factors. The relative ranking was used since the number of secreted vs non-secreted factors varied depending on tissue and mode of detection (type of array or RNA-sequencing). Differences in numbers of genes detected in each tissue is also the reason why the axes of each cross-tissue comparison show somewhat differing values for their distribution. For example, the muscle-to-adipose tissue y-axis possesses a higher numeric range due to the combination of more genes detected in muscle, as well as the strong cross-tissue correlation of non-secreted factors specific for this axis. Given that the sum of the -ln(pvalue) is directly proportional to the Ssec score, regardless of the range shown below each axis, the interpretation of the enrichment of secreted vs non-secreted factors remains constant for every comparison. Most cross-tissue axes show enrichment for secreted factors at the higher significance levels (top-right region of the graph).

SUPPL FIG 6 - LCN5 DOSE-DEPENDENT TREATMENT, related to Figure 4: C2C12 myotubes were treated overnight (16hrs) with indicated doses of LCN5 then qPCR probed for the genes listed. N=4 All data presented as mean ± SEM *p<0.05, **p<0.01

SUPPL FIG 7 – QUANTIFICATION OF LCN5 IN COCULTURE EXPERIMENTS, related to Figure 4I-K: 3T3L Adipocytes used in Fig 4I-K were quantified for the transcript abundance of Lcn5 using qPCR. N = 4, All data presented as mean ± SEM *p<0.05

SUPPL FIG 8 – PLASMA ADENO PROTEIN MEASUREMENTS, related to Figure 5: Western blots ad corresponding quantifications for plasma measurements of Ad-LCN5 (A), Ad-NOTUM (B).

SUPPL FIG 9 – ADENO-LCN5 MICE ON NORMAL CHOW DIET ITT AND GTT, related to Figure 5: Mice administered Ad-GFP or Ad-LCN5 for 9 days were subjected to an oral glucose or insulin tolerance test, in a similar fashion as in **Fig 5C-F**.

SUPPL FIG 10 – AAV-LCN5 COHORT EXPREIMENTS, related to STAR Methods section *Adeno-associated virus models*: Mice administered AAV-GFP or AAV-LCN5 and HF/HS diet for time-courses indicated were evaluated for body weight, composition, insulin and glucose tolerance.

SUPPL FIG 11 – TISSUE-WIDE GFP BLOTS TO ASSESS LCN5 TARGETS, related to Figure 4I-K and Figure 5: Indicated tissues from mice in Suppl. Fig. 10 were immuoprobed for GFP to identify target tissues of LCN5. Below the same Plantaris and Soleus muscles were immuoprobed for Noq7 to verify fiber type.

SUPPL FIG 12 – CONCORDANCE OF SSEC BETWEEN HMDP AND STARTNET, related to Figure 6: S_{sec} scores for all matching datasets between the two populations are plotted. The

strategy is presented in A and data points in B, where r, and pvalues indicated significant concordance.

SUPPL FIG 13 – NOTUM POOLED EXPERIMENTS FOR METABOLIC CAGES, related to Figure7: Pooled replicates from 3 experiments of metabolic chambers from mice administered Ad-GFP or Ad-NOTUM aggregated (**A-F**) or presented as time-series data (**G, H**)

SUPPL FIG 1 – PERMUTATION TESTING AND OVERVIEW FIGURE:

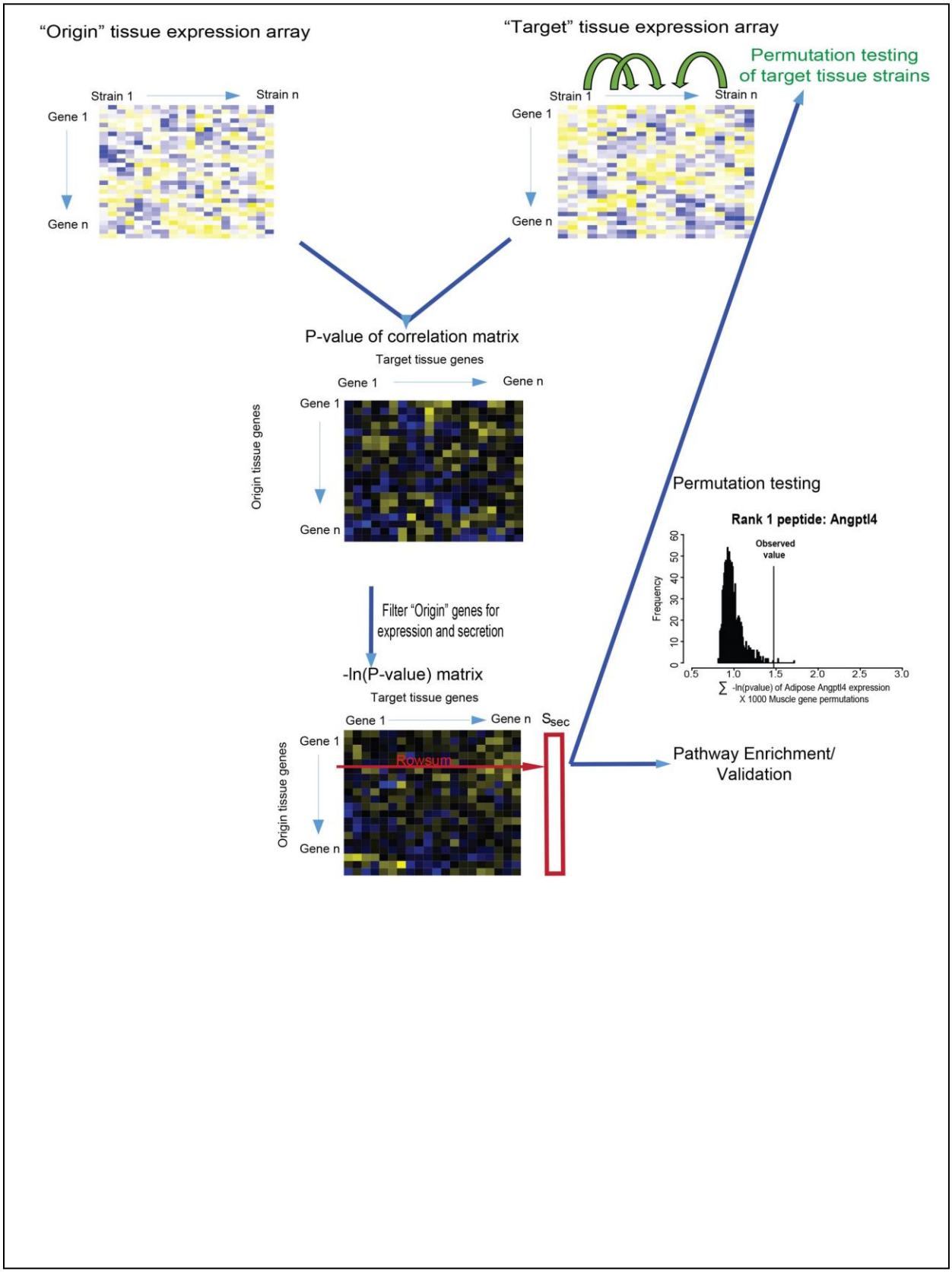

SUPPL FIG 2 – BIOGPS ARRAYS USED TO INFER TISSUE SPECIFICITY

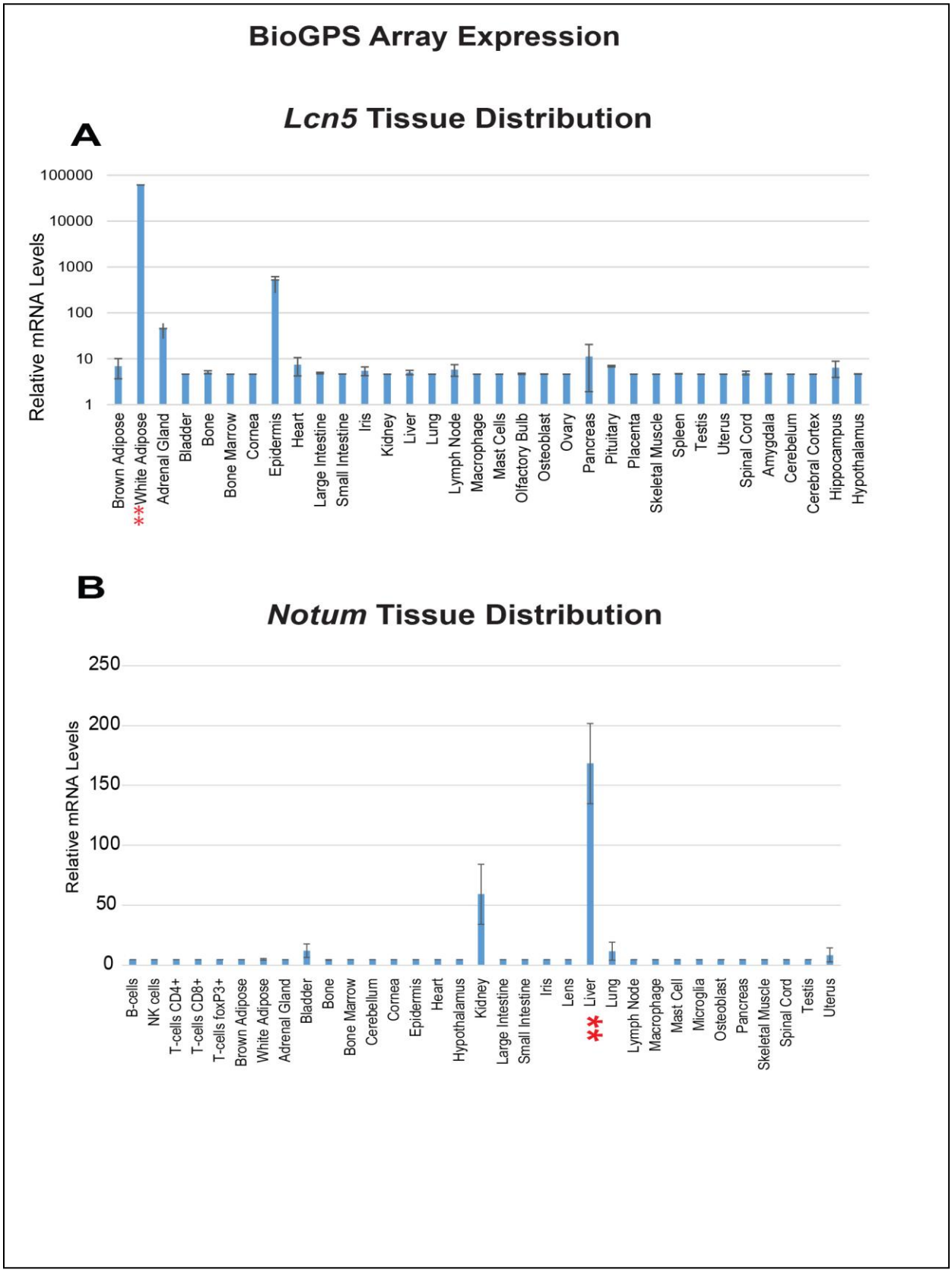

SUPPL FIG 3 – SEX DIFFERENCES AMONG SSEC SCORES

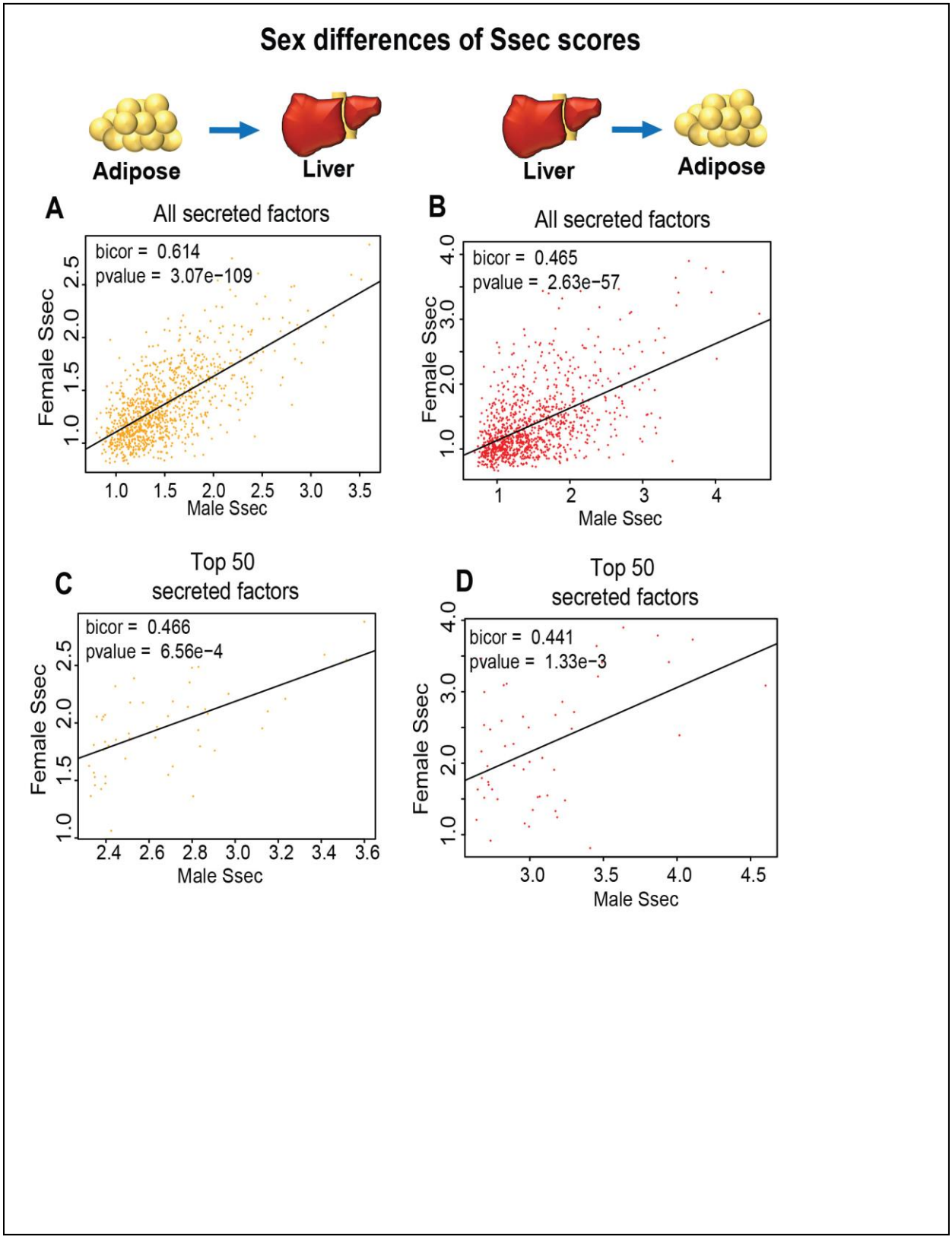

SUPPL FIG 4 – ALTERNATIVE STRATEGIES TO CROSS-TISSUE CORRELATIONS

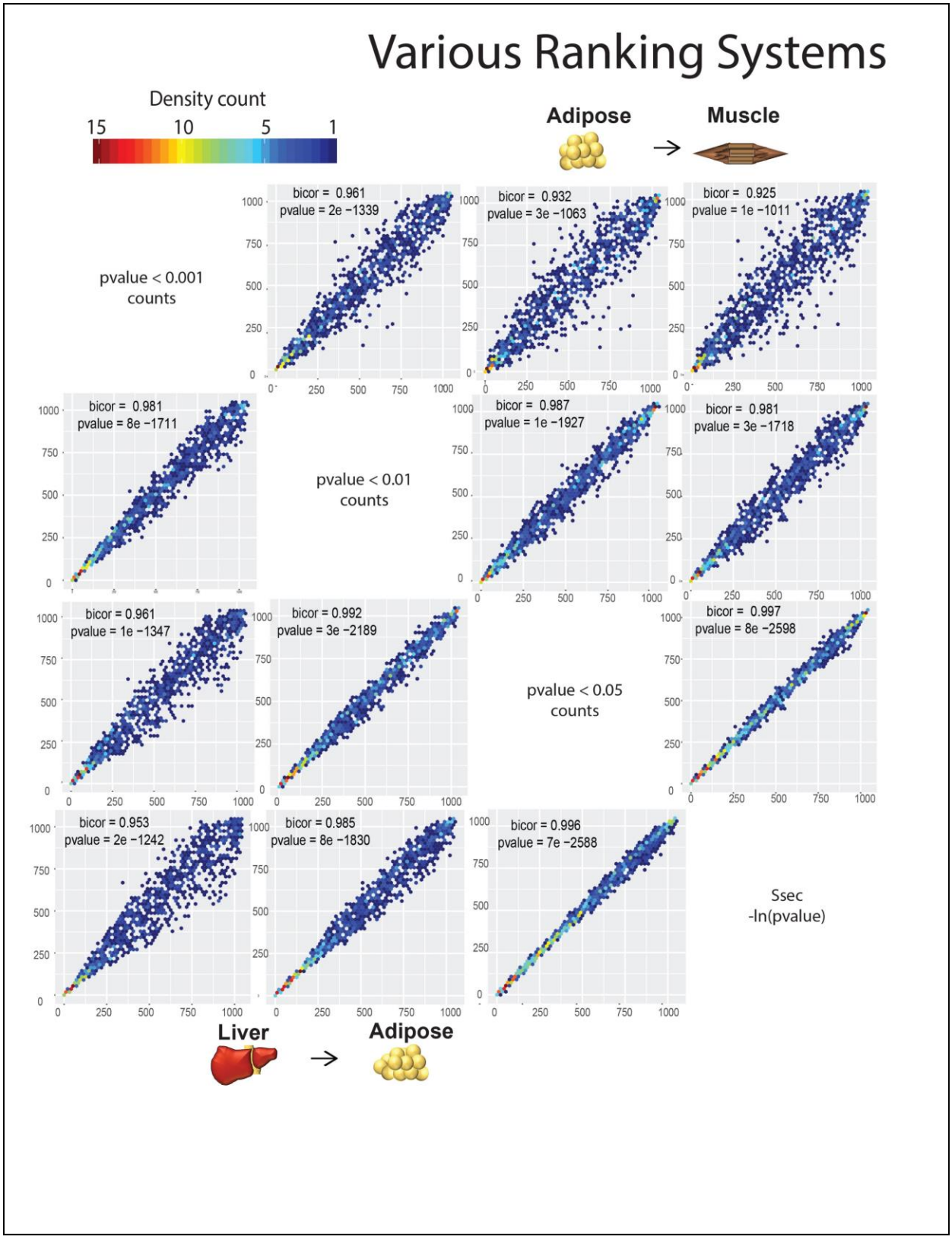

SUPPL FIG 5 – QQPLOTS FOR ENRICHMENT OF SECRETED FACTORS

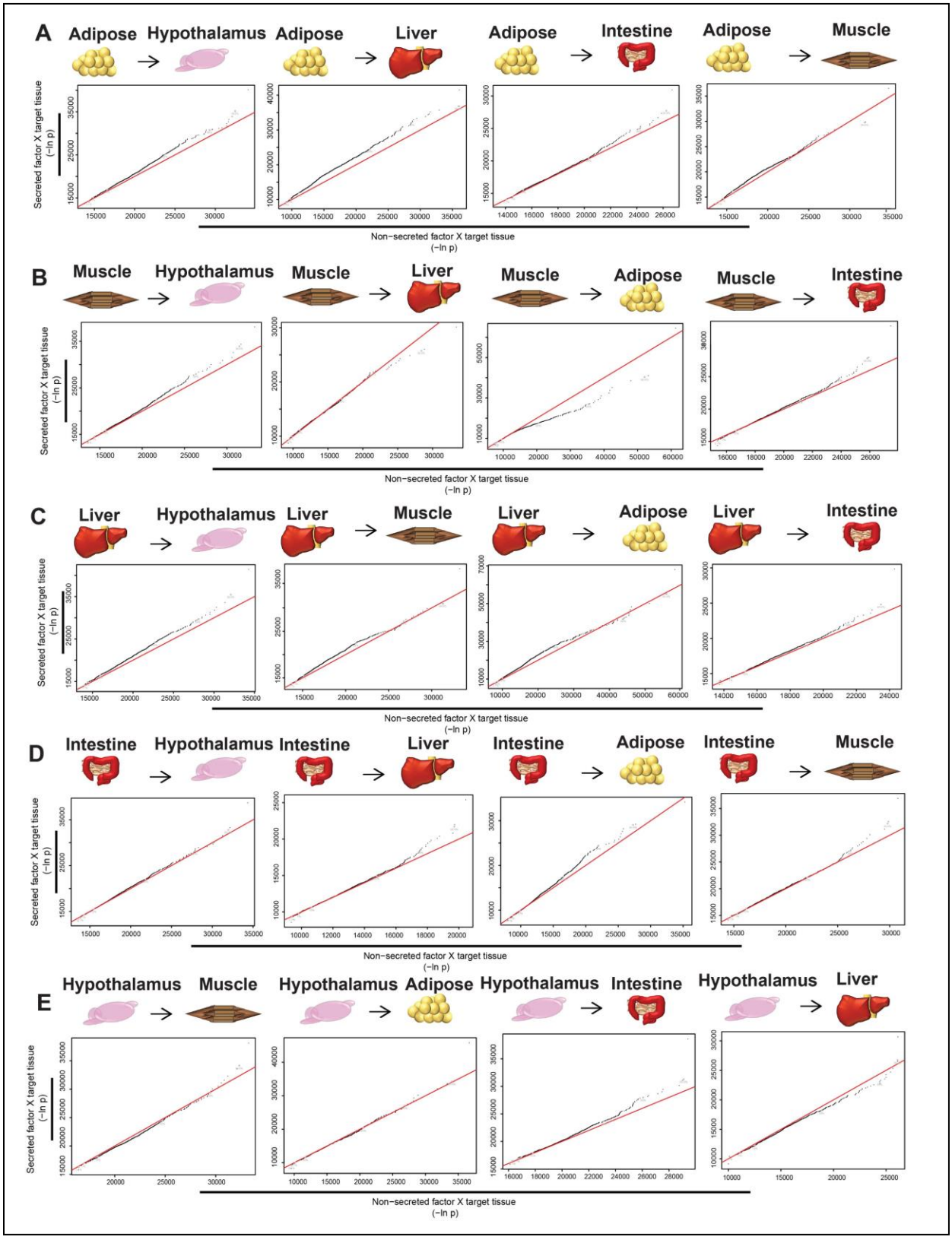

SUPPL FIG 6 - LCN5 DOSE-DEPENDENT TREATMENT

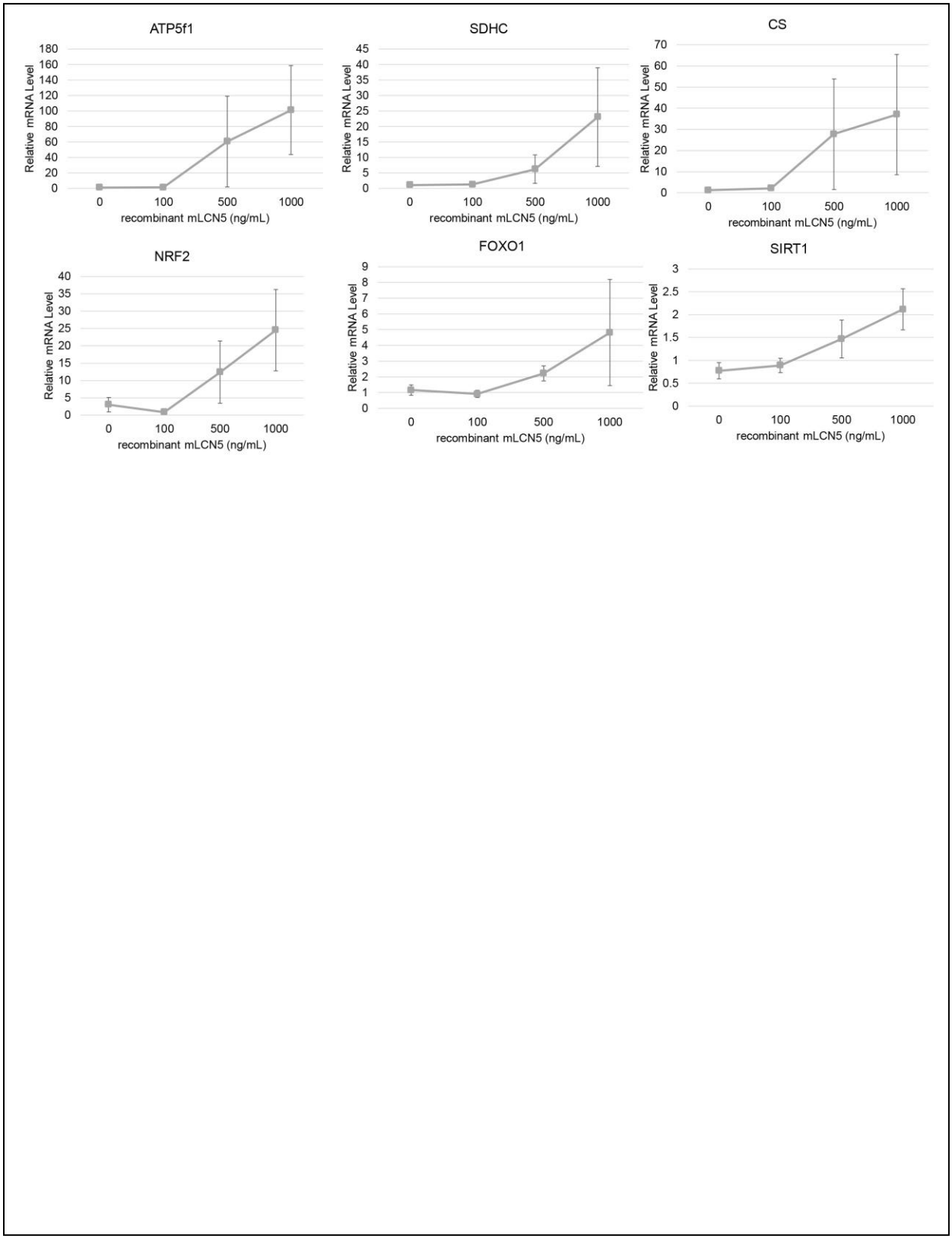

SUPPL FIG 7 – LCN5 MRNA QUANTIFICATION IN COCULTURED MYOTUBES

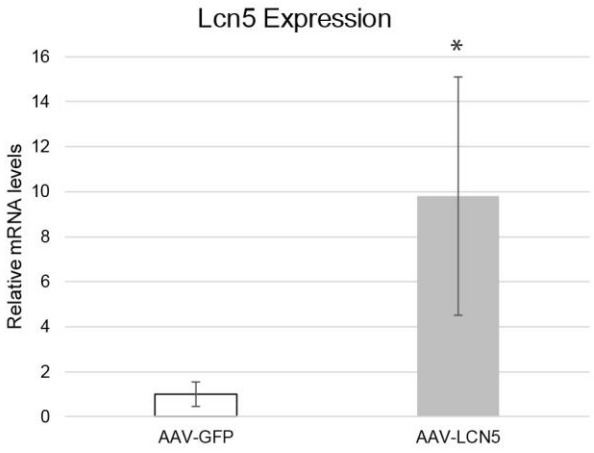

SUPPL FIG 7 – PLASMA ADENO PROTEIN MEASUREMENTS

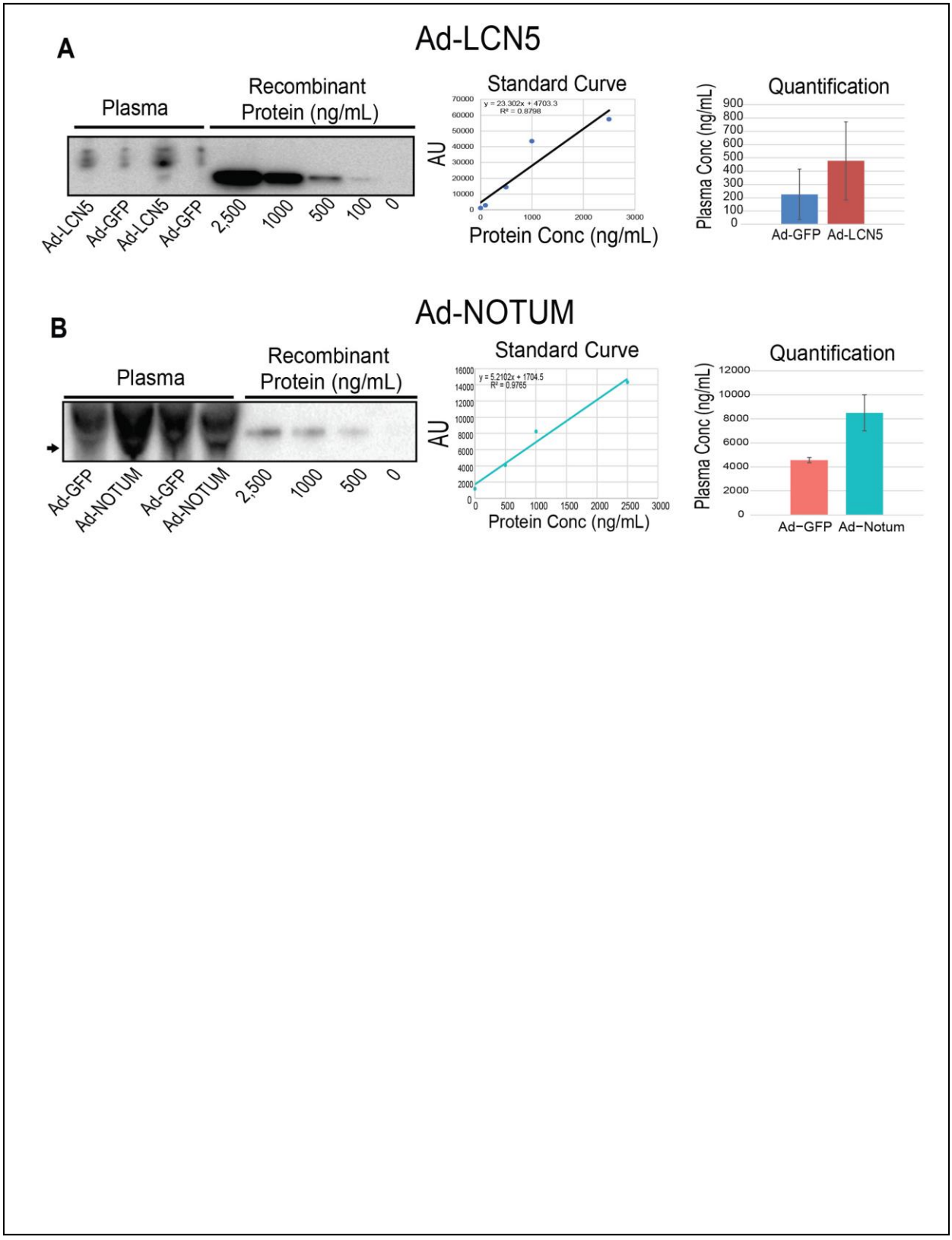

SUPPL FIG 9 – ADENO-LCN5 MICE ON NORMAL CHOW DIET ITT AND GTTSUPPL

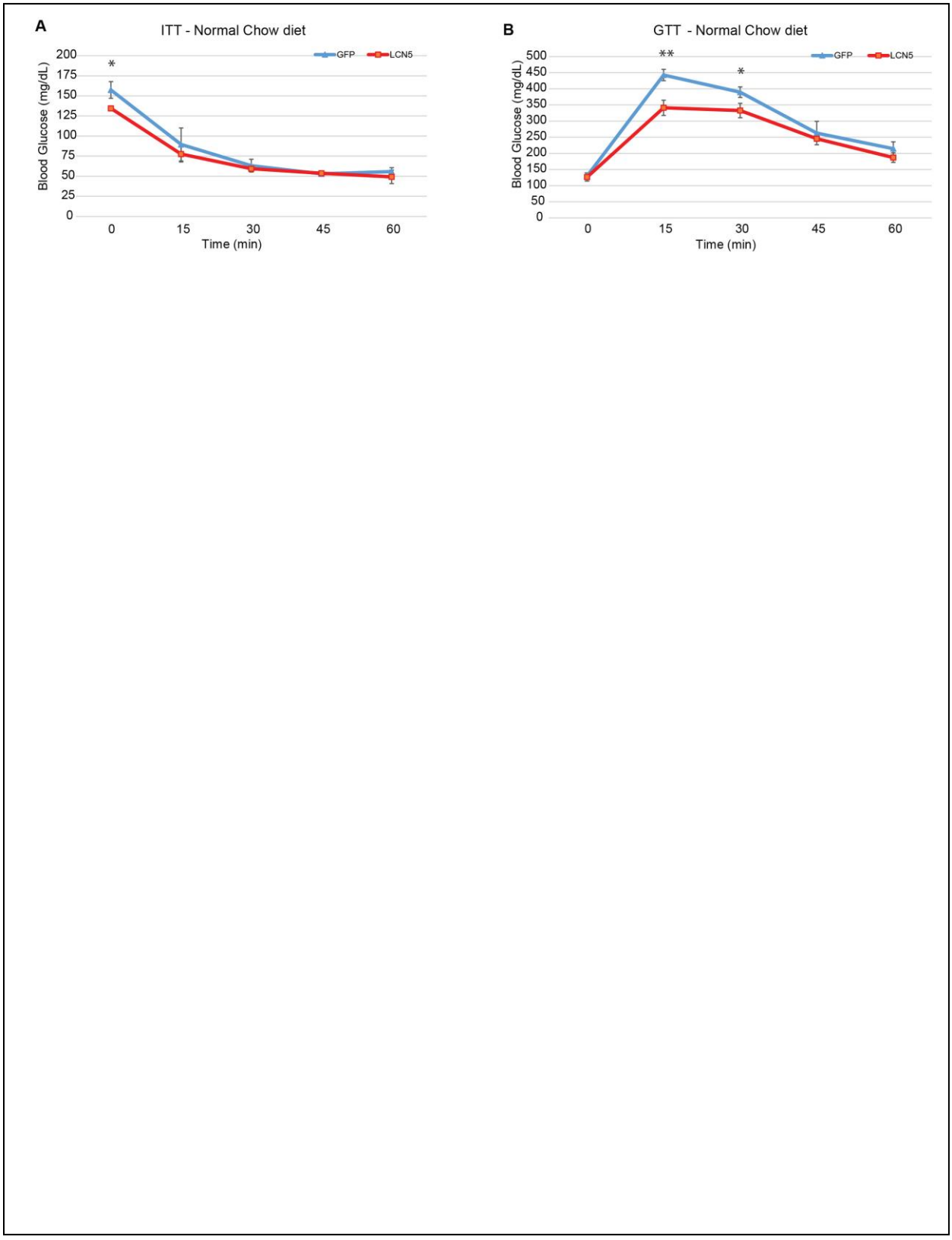

SUPPL FIG 10 – AAV-LCN5 COHORT EXPREIMENTS

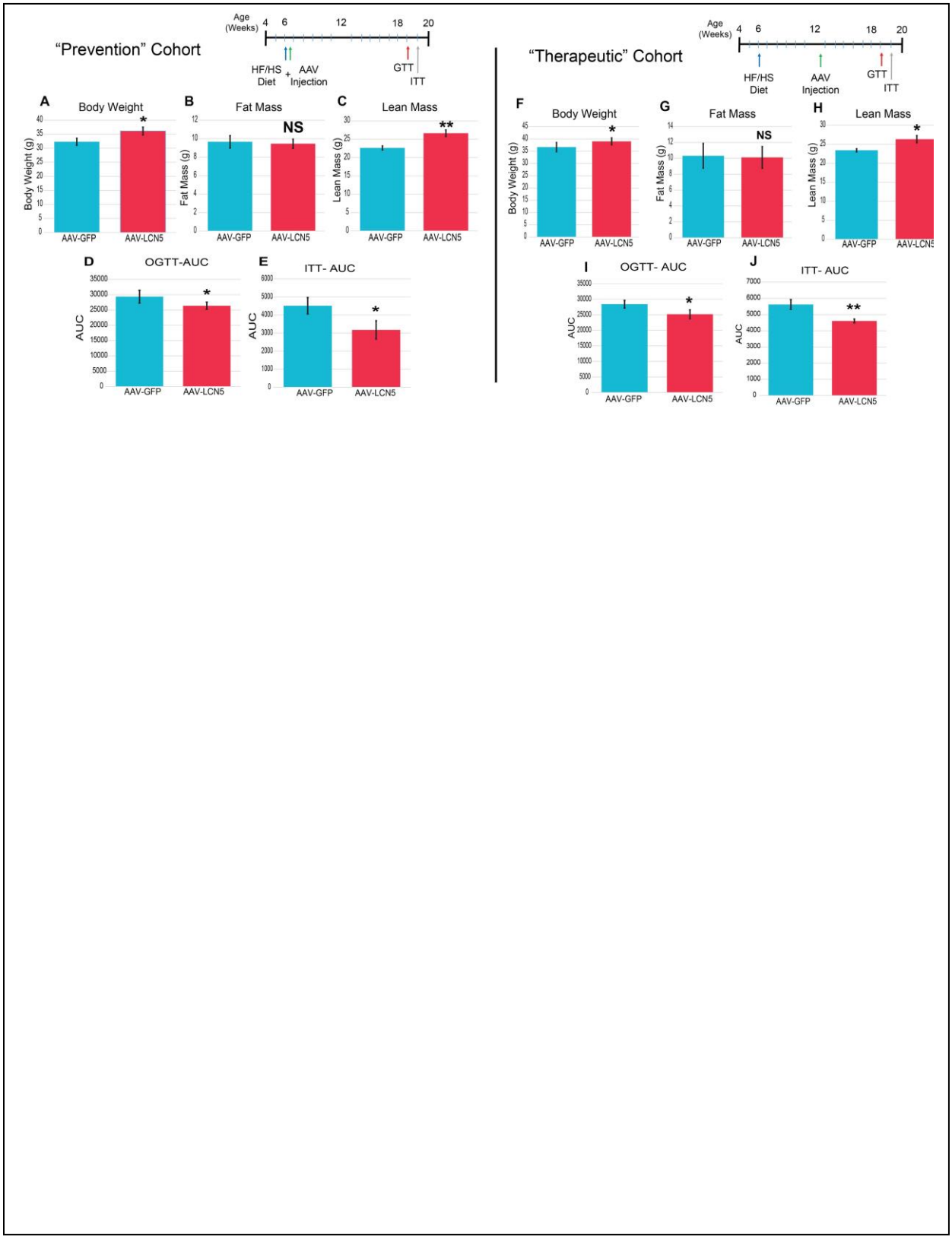

SUPPL FIG 11 – TISSUE-WIDE GFP BLOTS TO ASSESS LCN5 TARGETS

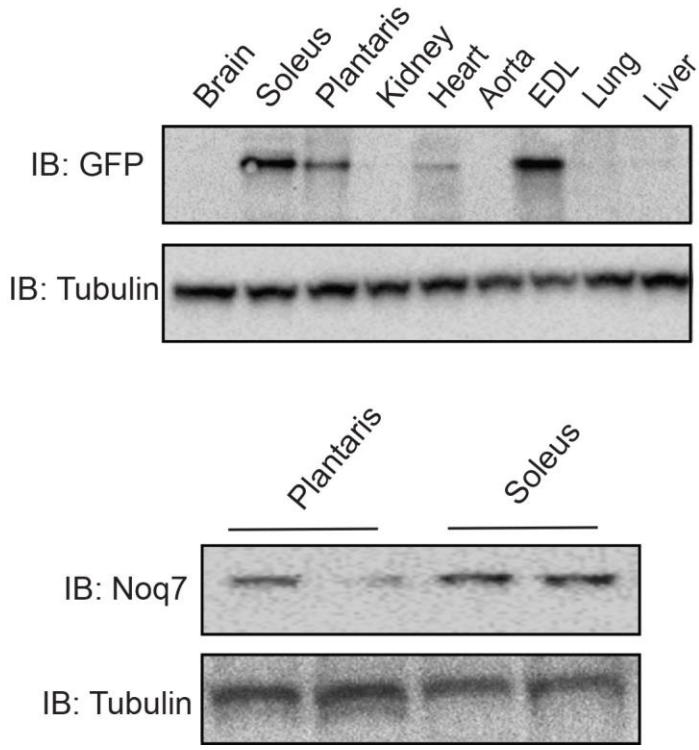

SUPPL FIG 12 – CONCORDANCE OF SSEC BETWEEN HMDP AND STARTNET

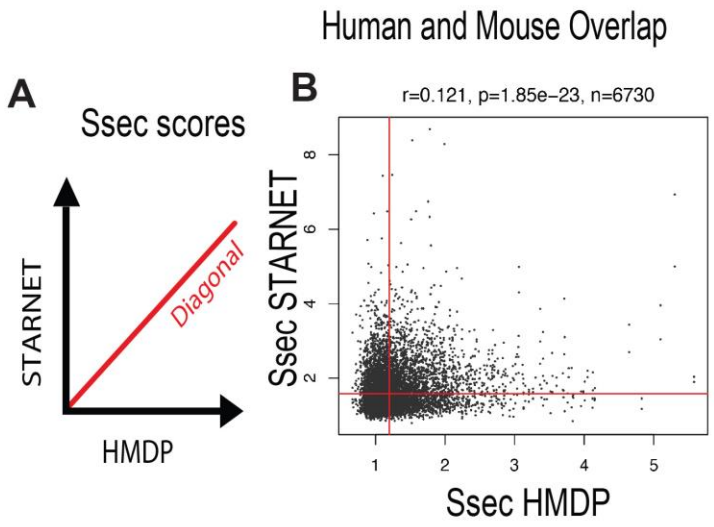

SUPPL FIG 13 – NOTUM POOLED EXPERIMENTS FOR METABOLIC CAGE